EXPERIMENTAL AND COMPUTATIONAL ANALYSIS OF A RINGING PLATE PYROSHOCK TEST SYSTEM

A THESIS SUBMITTED TO
THE GRADUATE SCHOOL OF NATURAL AND APPLIED SCIENCES
OF
MIDDLE EAST TECHNICAL UNIVERSITY

BY

BAHADIR GÜRSOY

IN PARTIAL FULFILLMENT OF THE REQUIREMENTS
FOR
THE DEGREE OF MASTER OF SCIENCE
IN
AEROSPACE ENGINEERING

JANUARY 2021

Approval of the thesis:

EXPERIMENTAL AND COMPUTATIONAL ANALYSIS OF A RINGING PLATE PYROSHOCK TEST SYSTEM

submitted by **BAHADIR GÜRSOY** in partial fulfillment of the requirements for the degree of **Master of Science in Aerospace Engineering, Middle East Technical University** by,

Prof. Dr. Halil Kalıpçılar
Dean, Graduate School of **Natural and Applied Sciences** ________________

Prof. Dr. İsmail H. Tuncer
Head of the Department, **Aerospace Engineering** ________________

Assoc. Prof. Dr. Tuncay Yalçınkaya
Supervisor, **Aerospace Engineering, METU** ________________

Examining Committee Members:

Prof. Dr. Altan Kayran
Aerospace Engineering, METU ________________

Assoc. Prof. Dr. Tuncay Yalçınkaya
Aerospace Engineering, METU ________________

Prof. Dr. Demirkan Çoker
Aerospace Engineering, METU ________________

Assoc. Prof. Dr. Ercan Gürses
Aerospace Engineering, METU ________________

Assoc. Prof. Dr. Cihan Tekoğlu
Mechanical Engineering, TOBB ETÜ ________________

Date: 27.01.2021

I hereby declare that all information in this document has been obtained and presented in accordance with academic rules and ethical conduct. I also declare that, as required by these rules and conduct, I have fully cited and referenced all material and results that are not original to this work.

Name, Last name : Bahadır Gürsoy

Signature :

ABSTRACT

EXPERIMENTAL AND COMPUTATIONAL ANALYSIS OF A RINGING PLATE PYROSHOCK TEST SYSTEM

Gürsoy, Bahadır
Master of Science, Aerospace Engineering
Supervisor : Assoc. Prof. Dr. Tuncay Yalçınkaya

January 2021, 83 pages

Spacecraft are exposed to severe mechanical loads, including random and periodical vibration, acoustic loads, sinusoidal shock, and pyroshock during their trip to orbit. Such loads usually develop due to a separation event through the activation of pyrotechnic devices and might be transmitted throughout the entire structure and seriously affect electronics components' service performance. It is crucial to study whether the instruments would resist such a harsh environment. Different instruments are validated with various experimental setups, most of which are open-loop systems. Therefore, due to the vulnerability and high cost of the space instruments, the designed experimental setups should be calibrated with dummy equipment to ensure the desired shock level is applied, which takes considerable time and effort. In this context, the current study investigates the potential of the explicit finite element method in designing a ringing plate pyroshock test system and the phase of calibration tests. In order to realize this, a set of preliminary finite element simulations are performed, and the design process of the ringing plate test system is presented. Various experiments are conducted with the designed and manufactured test bench. The obtained Shock Response Spectrum (SRS) responses are fitted to the explicit finite element simulations, which show good agreement after sensitivity analysis. Then the simulations are repeated with the dummy instrument using the

fitted parameters, and the potential of the numerical approach to predict a realistic response is discussed.

Keywords: Pyroshock, Mechanical Excitation, Impact Loading, Explicit Finite Element Analysis, SRS Curve.

ÖZ

BİR ÇINLAMA PLAKASI PİROŞOK TEST SİSTEMİNİN DENEYSEL VE HESAPLAMALI ANALİZİ

Gürsoy, Bahadır
Yüksek Lisans, Havacılık ve Uzay Mühendisliği
Tez Yöneticisi: Doç. Dr. Tuncay Yalçınkaya

Ocak 2021, 83 sayfa

Uzay araçları yörüngeye yolculukları sırasında rastgele ve periyodik titreşim, akustik yükler, sinüzoidal şok ve piroşok dahil olmak üzere ciddi mekanik yüklere maruz kalırlar. Bu tür yükler genellikle piroteknik cihazların aktivasyonu yoluyla bir ayrılma olayından dolayı gelişir ve elektronik bileşenlerin servis performansını ciddi şekilde etkileyebilir. Bu nedenle, ekipmanların böylesine sert bir ortama direnip direnmeyeceğini incelemek çok önemlidir. Çeşitli ekipmanlar birçoğu açık kontrol döngüsüne sahip deney düzenekleri ile doğrulanmaktadır. Bununla birlikte, ekipmanların kırılganlığı ve yüksek maliyeti nedeniyle, tasarlanan deney düzenekleri uygulanan şok seviyesinden emin olunması için kukla ekipmanlarla kalibre edilmelidir. Bu kalibrasyon süreci kayda değer bir zaman ve çaba gerektirmektedir. Bu bağlamda, mevcut çalışma, hem bir çınlama plakası piroşok test sisteminin tasarımı aşamasında hem de kalibrasyon testleri aşamasında açık sonlu elemanlar çözümünün potansiyelini araştırmayı amaçlamaktadır. Bunu gerçekleştirmek için bir dizi ön sonlu eleman simülasyonu gerçekleştirilmiş ve çınlama plakası test sisteminin tasarım süreci sunulmuştur. Tasarlanan ve üretilen test düzeneği ile çeşitli testler yapılmış ve elde edilen Şok Tepki Spektrumu (SRS) yanıtları, duyarlılık analizleri sonrası test sonuçları ile iyi bir uyum gösteren açık sonlu eleman analizi sonuçları ile karşılaştırılmıştır. Ardından test ile uyumlandırılan bu parametreler kullanılarak kukla ekipman ile analizler gerçekleştirilmiş ve numerik yaklaşımın test sonuçlarını doğru şekilde tahmin etme potansiyeli tartışılmıştır.

Anahtar Kelimeler: Piroşok, Mekanik Tahrik, Darbe Yüklemesi, Açık Sonlu Elamanlar Analizi, SRS Eğrisi

For everyone who dreams of space…

ACKNOWLEDGMENTS

Foremost, I wish to express my sincere gratitude to my supervisor, Assoc. Prof. Dr. Tuncay Yalçınkaya for his invaluable guidance and endless encouragement throughout the research. I especially thank him for his honest and instructive approach.

I also would like to thank jury members, Prof. Dr. Altan Kayran, Prof. Dr. Demirkan Çoker, Assoc. Prof. Dr. Ercan Gürses, and Assoc. Prof. Dr. Cihan Tekoğlu for their feedbacks on my thesis as jury members.

I would like to express my thanks to BIAS Engineering for giving me the opportunity to study in this area. I also wish to thank Aydın Kuntay and Ender Koç, who provide the base idea that initiates all the work presented in this thesis study.

I wish to acknowledge the endless support of my colleagues Burak Erdal and Ahmet Çağlayan.

I would like to express my thanks to my family, especially my parents Mualla, Selçuk, and my dear brother Bora for their encouragement.

Lastly, I would like to express my deepest gratitude to my love Aslı Aygün Gürsoy for her patience, respect, endless love, and guidance.

TABLE OF CONTENTS

LIST OF TABLES

TABLES

LIST OF FIGURES

FIGURES

LIST OF ABBREVIATIONS

ABBREVIATIONS

SRS – Shock Response Spectrum

FEM – Finite Element Method

SEA – Statistical Energy Analysis

DUT – Device Under Test

MIPS – Mechanical Impact Pyro Shock

Qual – Qualification Test

FA – Flight Acceptance

PF – Proto Flight

SDOF – Single Degree of Freedom

IP – In-Plane

OOP – Out-Of-Plane

SRSS – Squared Root of the Summation of Squared Values

CNRB – Constraint Nodal Rigid Body

CHAPTER 1

INTRODUCTION AND LITERATURE REVIEW

Space has been practically in our lives since the first human-made object entered space in the late 1940s. It has an increasing role in our daily life in the fields of global positioning systems, cell phones, communication, and weather forecast. Exploring space also utilizes the understanding of our existence and universe and the pioneers some of the most advanced technologies. However, it is one of the extreme environments at the same time. A spacecraft needs to withstand several complex loadings such as high gravitational loads, periodic and random vibrations, acoustic loads, pyrotechnic shocks together with the payload in the lunch period. After reaching space, it experiences very high-temperature gradients, high radiation levels, shocks from deploying mechanisms, and maneuver loads. Considering the high expenses of space programs and very demanding mass optimization requirements, all these extreme conditions create tough design challenges for engineers. Among the type of loadings and conditions, all kind of shock loadings become prominent due to highly complex nature and possibly fatal effects on aerospace structures.

1.1 Background Information and Methodology

1.1.1 Shock Definition

Among the different attempts to define shock loading, one of the most widely accepted definition is presented at the first Shock and Vibration Symposium in 1947 as “a sudden and violent change in the state of motion of the parts or particles of a body or medium resulting from a sudden application of a relatively large external force, such as blow or impact”[1]. Such a high-energy event that occurs in a short duration of time could cause damage to critical structures and devices such as civil engineering structures, military and civil vehicles, aircraft, and aerospace structures. It is convenient to define the "short duration" property of shock loading as "much shorter than the fundamental frequency of the system"[2]. It means that the system under shock loading responses freely since the excitation time is much shorter than the response time. Shock is complicated and oscillatory; it has frequency content up to 1 MHz for explosive-induced shocks[3]. Therefore, there is no easy way to measure the shock but measure the system's acceleration response. A typical shock loading has a duration smaller than 20 ms[4] and the amplitude of its acceleration response could be between several g's and hundreds of thousands of g's in specific cases. A typical acceleration response of a shock loading is presented in Figure 1-1.

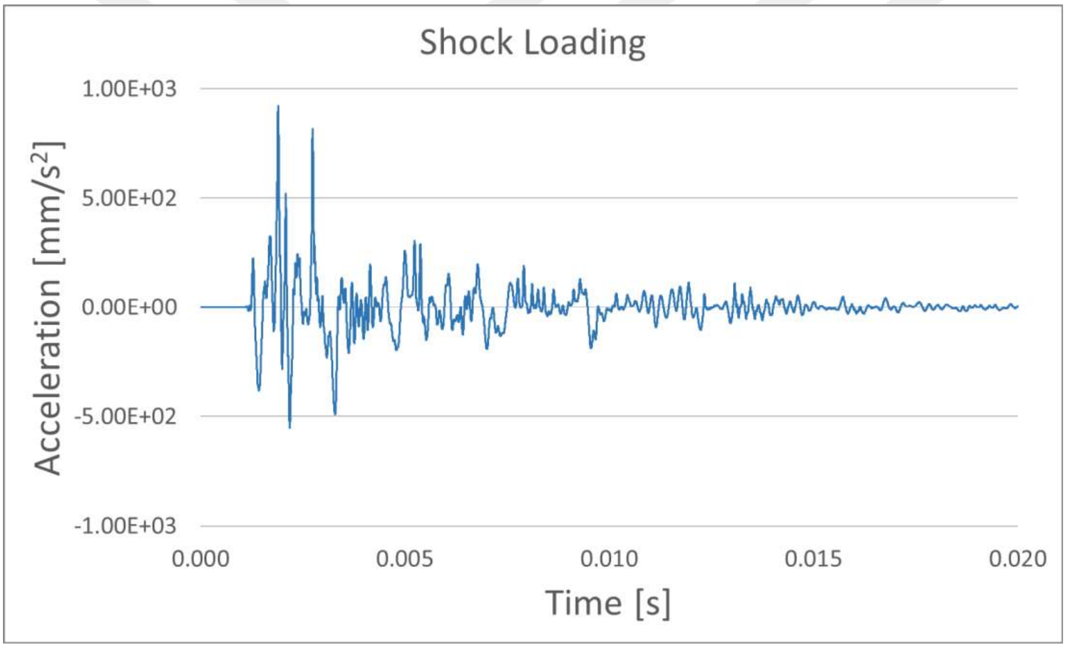

Figure 1-1. Typical acceleration response of a shock loading

As an alternative, the shock could be represented as a propagating mechanical wave in a structure or medium. Fundamental mechanical waves could be classified into three categories: Tension-compression waves, shear waves and flexural waves as presented in Figure 1-2.

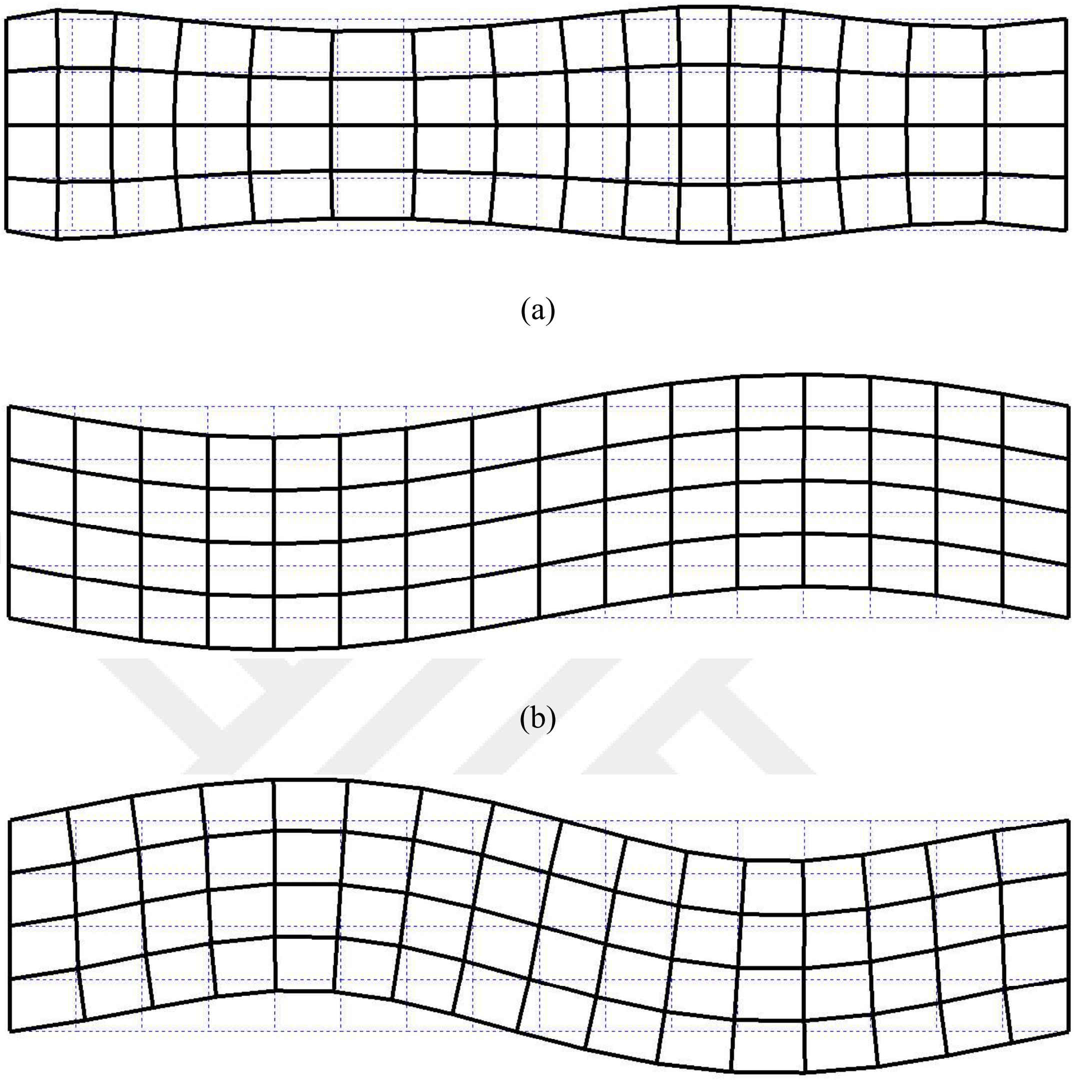

(a)

(b)

(c)

Figure 1-2. Schematic representations of waves[5]. (a) Tension – compression wave. (b) Shear wave. (c) Flexural wave

Structures exposed to a tension-compression wave deform parallel to the propagation direction, successive tension and compression regions occur. On the contrary, shear waves deform the structure in a direction perpendicular to wave propagation. Shear waves occur in relatively higher frequencies than tension-compression waves. Both types of mechanical waves are non-dispersive, i.e., their propagation speed does not change with the frequency, waves of different frequencies travel together without any phase shift, and the waveform does not deform as it propagates. On the other hand, flexural waves bend the structure, as the name emphasizes. It creates deformation both parallel and perpendicular to the propagation direction. They are dispersive so that their speed depends on the frequency of the specific wave, and their waveforms deform as the wave propagates.

1.1.2 Pyroshock and Pyrotechnic Devices

Pyro comes from the Greek word πῦρ (pyr), originally meaning fire, but it is used to relate something with explosives in today's engineering world. Pyrotechnics or pyrotechnic devices contain separate ready-to-use energy sources consisting of an explosive and an oxidizer together. Pyroshock, or pyrotechnic shock, is defined as the transient response of the structures, components, and systems due to the loading induced by the pyrotechnic devices attached to the structures[6]. In general, pyroshock moves in terms of linear elastic stress waves to the adjacent structures without plastic deformation, except when in the vicinity of the pyrotechnic devices. Pyroshock could have frequency content up to 1MHz, and it could reach amplitude levels up to 10,000 g’s and more.

Pyrotechnic devices have been commonly used in the aerospace industry for quite a long time. They have been used substantially on aerospace vehicles to carry out a significant number of work functions such as cutting, separation, pressurization, valving, electrical switching, personnel ejection as well as emergency and lifesaving applications. The usage of pyrotechnics is advantageous compared with the other release devices based on non-explosive actuators thanks to low volume-weight ratio, high reliability, instantaneous operation with simultaneity, long-term storage capability, and low cost. For detailed overviews on such devices, one can refer to old NASA reports (see, e.g. [7] and [8]).

Even though pyrotechnic devices have various advantages, the induced pyroshocks might result in catastrophic failure of the nearby optical and electrical components sensitive to high-frequency energy. This failure is a crucial concern, and it might eventually result in the failure of the flight. According to a report of Moening on the cause of failure on space programs between 1960 – 1982, of the 85 observed failures, 84% are directly or potentially related to pyroshock induced problems [9].

Due to the high potential of causing fatal problems, many researchers have studied pyroshocks in the literature. However, it is still a challenging issue to measure pyroshock and simulate it in order to assess the vulnerability of a device exposed to pyroshock. Experimental and numerical analyses exist in the literature addressing propagation of pyroshocks and their effects. (see [10] for a review). The studies have mostly focused on the experimental approaches where the pyroshock is simulated on test various test benches. Both experimental and numerical methods in the literature are explained later in this chapter.

1.1.3 Categorization of Pyroshocks

Pyroshocks could be divided into three categories based on frequency content and acceleration level of shock categories to investigate in detail and construct the methods and procedures: near-field, mid-field, and far-field. There are several standards for assessments of pyroshocks, but the most widely accepted ones are NASA-STD-7003A[11], IEST RP Pyroshock Test Technique[12], and MIL-STD-810H Method 517[2]. They all agree on the categorization of pyroshock, which is presented in Table 1.1.

Table 1.1 Pyroshock Categories

Category Name	Frequency Content [Hz]	Acceleration Levels [g]
Near-Field	>10,000	>10,000
Mid-Field	3,000 – 10,000	1,000-10,000
Far-Field	<3,000	<1,000

Near-field pyroshock occurs in the only very vicinity of the pyrotechnic device itself. Different from other categories, near-field pyroshocks tend to create plastic deformation and failures on structural elements. The response of the structure is governed by the material stress wave only.

Mid-field pyroshock is observed near the detonation point. They hardly create plastic deformation, and the response of the structure is governed by material stress wave and the resonance response of the structure together.

Only the structure's resonance response governs far-field pyroshock loading, and the effect of the detonation stress wave is almost completely lost. Those kinds of loadings are observed far from the detonation point, and practically no deformation occurs on structural elements. However, brittle materials and electronic and optical devices are still vulnerable.

1.1.4 Shock Response Spectrum (SRS) Method

Acceleration measurements obtained from high-frequency oscillatory shock loadings, such as pyroshocks, are almost impossible to use and evaluate in the time domain. They are chaotic and complex, and their frequency content comprises a large spectrum. Therefore, in 1932 Biot proposed a method for complex shock loadings known as Shock Response Spectrum (SRS)[13]. His work is initially suggested to study earthquakes' damage potential on civil structures such as tall buildings. Ever since, the shock response spectrum is used to evaluate the damageability of various transient shock loadings, including pyroshock. Main shock environment qualifications standards such as MIL-STD-1540C and MIL-STD-810H presented requirements for SRS curves for different environments. In 2012, Irvine[14] pointed out the methodology for applying the shock response spectrum to aerospace structures. Furthermore, SRS is preferred in a lot of different recent works in literature (see, e.g. [15-27])

Shock Response Spectrum presents a curve that consists of the measurements of peak accelerations of a set of single-degree-of-freedom (SDOF) systems over a frequency range under applied transient shock loading (Figure 1-3). Each SDOF system is connected to the same base where the excitation is imposed as acceleration. Every

SDOF system has adjusted such that it represents a natural frequency in the domain. All systems together cover the entire frequency spectrum needed to be examined.

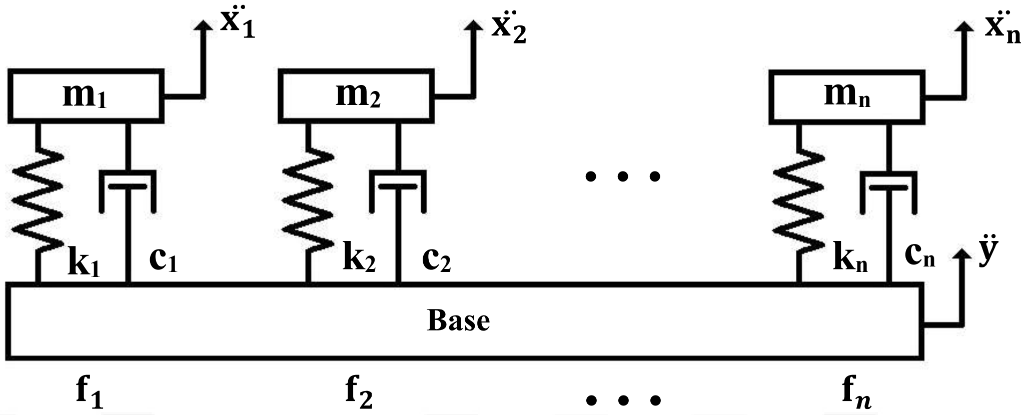

Figure 1-3. Schematic representation of SDOF systems

Shock Response Spectrum represents the maximum response of structure as if the system has natural frequencies at every point throughout a frequency range. Same acceleration – time data is used as input for every SDOF system. Peak acceleration of the SDOF system is collected, and this information is transferred to the SRS curve as a point. This peak acceleration is collected at the resonance frequency with a 3dB-bandwidth, i.e., the bandwidth between the -3dB points (half-power-gain points) straddling the resonance frequency. The quality factor (Q) of the SDOF system, which is defined as the resonance frequency divided by the resonator bandwidth, is taken 10 for the calculation. Figure 1-4 and Figure 1-5 show an example. A relatively basic shock loading, 11 ms 55 G half-sinus shock loading, is applied to the base plate as an input. The response of three different SDOF systems, which have resonant frequencies at 30Hz, 80Hz, and 140Hz, are calculated in the time domain. Lastly, absolute maximum acceleration values of responses, 55g, 82g, and 70g, respectively, are marked in the SRS graph. This acceleration data could be a positive peak, negative peak, or absolute peak. The choice of it gives the name to the method such as positive shock response spectrum or maximum shock response spectrum etc.

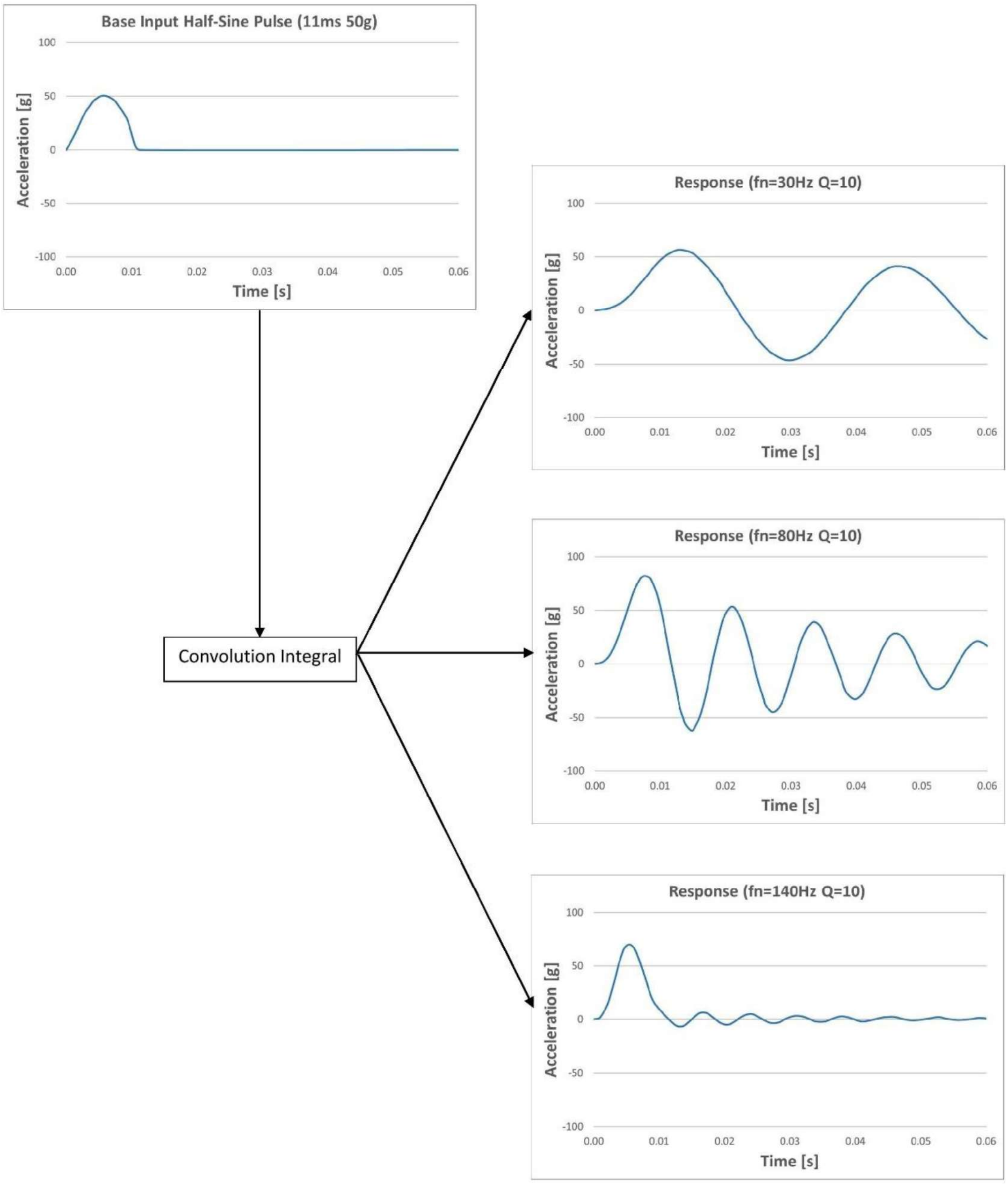

Figure 1-4. Calculation of peak responses on SDOF systems[14]

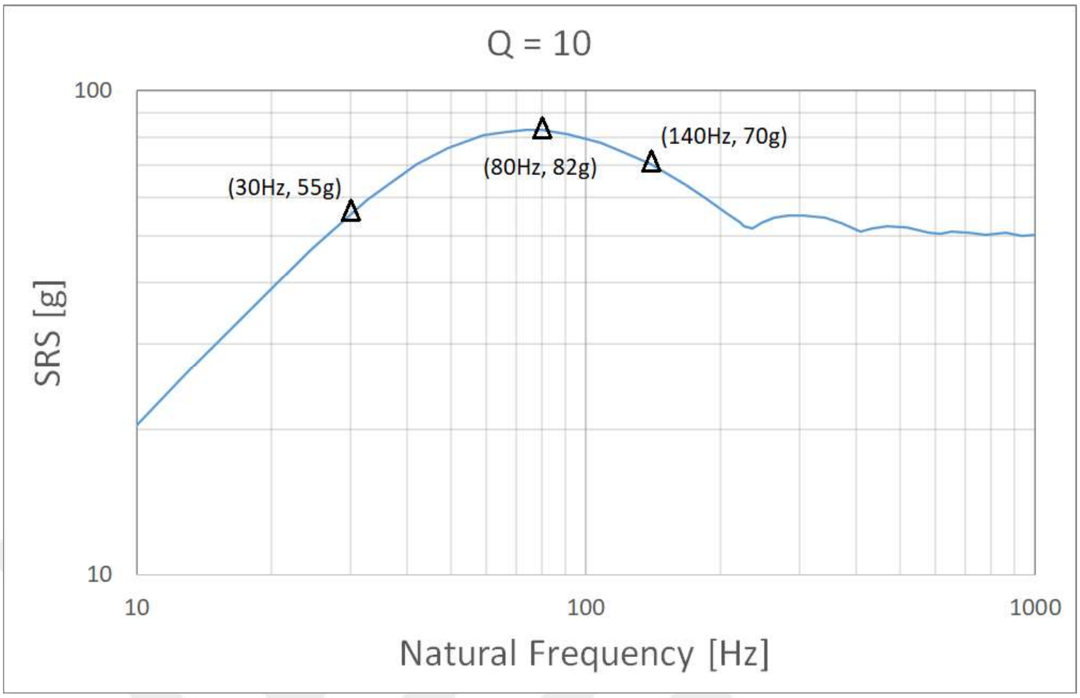

Figure 1-5. Calculated SRS curve[14]

Damping is taken as 5% of critical damping, which corresponds to a quality factor of 10. It is kept constant throughout the frequency range. Although the method permits any set of frequencies, typically a proportional bandwidth is preferred for SRS calculation. SRS curves could be divided into two regions, namely, ramp region and plateau region. The frequency which distinguishes the two regions is called knee frequency. However, the transition for some SRS curves is smooth and the exact transition frequency is not clear as in Figure 1-5.

Irvine[14] presents a complete derivation of the SRS method, starting from Newton Second Law applied to a free-body diagram of an SDOF system based on convolution integral.

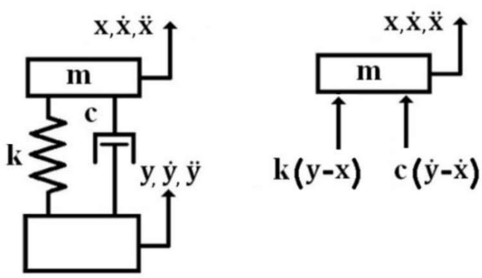

Figure 1-6. SDOF system and corresponding free body diagram of the mass

When forces are summed up on the FBD in Figure 1-6;

$$c(\dot{y}-\dot{x})+k(y-x)=m\ddot{x} \tag{1}$$

Now let us introduce $z=x-y$ and rewrite the equation.

$$-c\dot{z}+kz=m\ddot{z}+m\ddot{y} \tag{2}$$

$$-m\ddot{y}=m\ddot{z}+c\dot{z}+kz \tag{3}$$

Also, note that;

$$\omega_n^2=\frac{k}{m} \tag{4}$$

$$2\xi\omega_n=\frac{c}{m} \tag{5}$$

Substituting (4) and (5) into (3);

$$\ddot{z}+2\xi\omega_n\dot{z}+\omega_n^2 z=-\ddot{y} \tag{6}$$

Since for a general case $\ddot{y}$ could be any function, (6) has no close-form solution. A convolution integral approach is used to obtain the solution. The result of the convolution integral is presented in (7). A complete derivation could be found in the work of Irvine[14].

$$\begin{aligned}\ddot{x}_i = 2e^{-\xi\omega_n\Delta t}\cos(\omega_d\Delta t)\ddot{x}_{i-1} - e^{-2\xi\omega_n\Delta t}\ddot{x}_{i-2} + 2\xi\omega_n\Delta t\ddot{y}_i \\ + \omega_n\Delta t e^{-\xi\omega_n\Delta t}\left\{\left[\frac{\omega_n}{\omega_d}(1-\xi^2)\right]\sin(\omega_d\Delta t)\right. \\ \left. - 2\xi\cos(\omega_d\Delta t)\right\}\ddot{y}_{i-1}\end{aligned} \tag{7}$$

where;

ω_d is the damped resonance frequency of the system

subscription *i* represents the ith SDOF system in the frequency band

Equation (7) is calculated at every resonant frequency in the spectrum to construct the SRS curve.

1.1.5 Shock Verification Process

A significant set of dynamic loads exists among the loads that aerospace structures need to withstand, including pyroshocks, acoustic vibration loads, random and periodic vibrations, etc. These harsh loads create a challenging engineering task for optimized designs considering a limited weight budget for the structure, which is the usual case for aerospace structures. Furthermore, considering the expenses of space programs, it is evident that a very comprehensive testing and qualification process needs to be followed to minimize the failure risks.

According to MIL-STD-7003A[6], pyroshock test phases could be evaluated in different tests regarding different aims. They are classified as Qualification Tests(Qual), Flight Acceptance Tests(FA), and Protoflight Tests(PF).

Qual test is performed in order to check whether the considered system or instrument could withstand the necessary pyroshock environment or not. It has the most severe loading requirement among the test types. Thus, it is the one used to evaluate design integrity.

Ideally, an FA test is needed for every manufactured instrument and system planned to be mounted on an aerospace vehicle. An FA test's primary purpose is to check any production or craftsmanship error for a device that already passes the qual test. Therefore, loading in FA tests is lower than a qual test.

Protoflight test is an alternative of qual and FA test when there is limited equipment or system available. The PF test's loading level is equal to the qual test, and it unites the purpose of the qual and FA test within a single test.

Siam[28] summarizes the necessary shock tests, including pyroshock and shock loads in an aerospace vehicle's service life as shown in Figure 1-7.

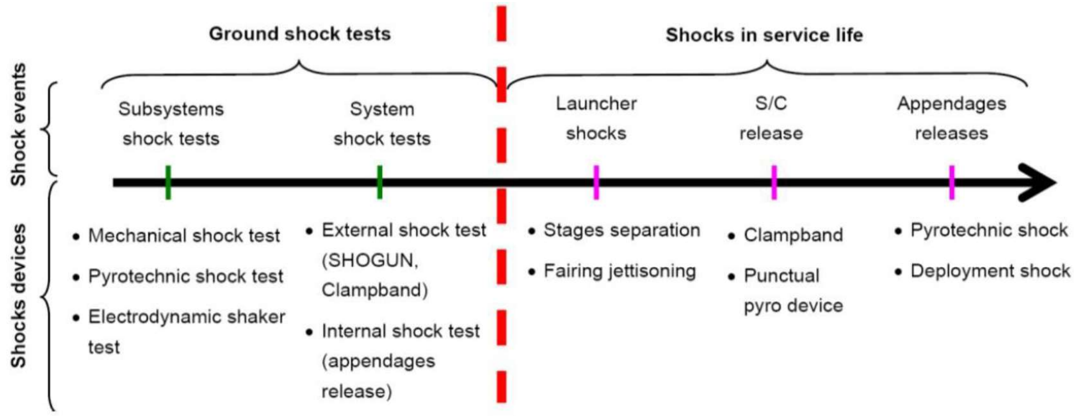

Figure 1-7. Shock tests and shock loads in the service life of an aerospace vehicle [28]

For a successful design, system, sub-system, and equipment level, pyroshock tests are vital. Ideally, those tests could be performed with real structures and pyrotechnic devices for both qual and FA tests. However, several problems occur in practical applications, such as lack of high-fidelity structure in early design phases, budget and time limitations, etc. It is common to use alternative pyroshock simulation methods, including mechanical-impact tests and commercial shaker tests where applicable and numerical simulations.

1.2 Experimental and Numerical Pyroshock Simulation Methods

For several decades, experimental pyroshock simulations are the main verification methods due to the complex and chaotic nature of the pyroshock. Moreover, pyroshocks vary substantially among different pyrotechnic devices. The situation seems to be more severe when it is considered that pyroshocks contain frequency content up to 1MHz and shock levels up to several hundred thousand g's. The most reliable option is performing a full-scale test with real pyrotechnic devices at the system and sub-system levels. However, it could be a proper strategy for final verification of the whole system in practical applications but not for instrument and sub-system level design iterations. Using real pyrotechnic devices is quite expensive and time-consuming to be beneficial for the latter. Thus an alternative way is an experimental simulation of pyroshock. It means to create a loading that mimics the real pyroshock loading a structure is exposed during its service life. Those methods are not as accurate as full-scale tests. However, they are used in various studies and aerospace laboratories [29] thanks to several advantages discussed later in this section.

For shock verification, a time and budget effective alternative to experimental methods are numerical simulations. Several techniques could be employed in order to replace the experimental ones. This replacement could be in terms of performing analysis of instrument or system for a defined pyroshock loading as well as a supplementary numerical analysis to reduce experimental test number as in this study. Although numerical simulation tools and methods are not as mature as experimental methods, they are still promising if the details of the methods are studied and limitations are specified.

1.2.1 Experimental Methods

Different experimental approaches and test systems are proposed in the pyroshock verification process of systems, sub-systems, and instruments. The type of method and choice of the test system depends on several parameters. They include but are not limited to the type of the device-under-test (DUT) such as instrument, sub-system, etc., pyroshock categories, the purpose of the test and timing in the project, i.e., early design iteration or final verification of a mature design. These parameters lead to a wide range of test system and method configuration. Some systems use "real" pyrotechnic devices to create pyroshocks. Others "simulate" the pyroshocks by other methods such as releasing instant strain energy with a laser beam or using a metal-to-metal impact etc. Another critical point is the capability of the test system in terms of the variety of DUT, i.e., whether the system needs to be capable of testing only one instrument or different types of instruments.

Classification of these methods and test systems is necessary in order to analyze and understand them correctly. Every system has its advantages and disadvantages, limitations, and application range as well. Jonsson[30] preferred to divide experimental test systems into categories based on pyroshock categories (near, mid, and far-field pyroshock). However, Eriksson and Hansson[31] divided in terms of test system types such as electrodynamic shaker, ringing plate test system, etc. In his review Lee et al.[10] analyzed the methods subcategorized by excitation method as the author prefers to do in this study.

1.2.1.1 Explosive Excitation

Explosive-excited test systems are the only ones that use "real" pyrotechnic devices instead of somehow "simulating" the pyroshock with any other method. It is the most preferable method in terms of accuracy. They are capable of simulating all levels of tests, namely, instrument, sub-system, and system level, for near, mid, or far-field pyroshock environments. In explosive-excited setups, it is not hard to reach the desired frequency and magnitudes. It is the main reason that they are advised to use for near-field pyroshock tests where high acceleration and high frequency is necessary to verify structural integrity issues (see, e.g. [6,10,18]).

In commercial applications, instrument level test systems mainly consist of single or multiple plates hanged or placed on top of a table-like structure as presented in Figure 1-8.

Figure 1-8. Explosive-excited instrument level test systems[30]

Explosive is placed to one side of the plate, and the device under test (DUT) is mounted to the other side. By initiation of the explosive, a shock loading transferred to DUT. Although explosives are used as an excitation method, it is still a kind of “simulation” of real pyroshock loading since neither is it an actual pyrotechnic device nor is there a high-fidelity structure between DUT and shock source.

Although explosive-excited systems are preferred in terms of accuracy, several disadvantages limit their usage with system and sub-system level final verification tests and near-fields instrument-levels tests. The use of pyrotechnic devices is quite expensive and involves high safety risks (see, e.g. [15-17]). Furthermore, application for instrument level tests, since it is still a simulation of real pyroshock, a trial-and-error process is inevitable before the real test to achieve the correct pyroshock loading on DUT[32]. These calibration tests are performed with a dummy DUT for budget reasons. Since high cost and requirement of special permissions because of the safety risks, explosive-excited systems are preferable only for near-field tests. No other alternative exists due to very high g levels and frequency content over 100kHz, as mentioned before.

Apart from the instrument tests, the explosive-excited tests are the only option for full-scale system tests. They are performed mostly at the very final phase of projects and contains real pyrotechnic devices and high-fidelity or actual aerospace structures. Several initiation stages are simulated by firing multiple pyrotechnic devices in the correct order as they are fired in service life. Full-scale tests are performed for the qualification of whole systems within only two QA tests, as described in standarts[6]. Ott has mentioned in his work[33] that these tests are expensive, time-consuming, and requires special facilities.

Figure 1-9. A full-scale separation test of the forward skirt extension for the Ares I-X[34]

1.2.1.2 Mechanical Excitation

Mechanical excitation is widely used for pyroshock verification of different instruments as an alternative to using explosives (see, e.g. [6,10,16,19,20]). It could be utilized through metal-to-metal impact, pneumatically accelerated impact, or an electrodynamic shaker.

Standard shock test systems such as drop tables are not one of the preferable pyroshock simulation methods though they are widely used to verify other shock types. A drop table gives a significant amount of kinetic energy to DUT, which is converted to velocity. It creates excessive deformations and net change in velocity as oppose to pyroshock loads make almost no net change in velocity but creates high accelerations. Therefore, this type of test benches could not simulate correct pyroshock loadings and are not suitable for pyroshock verifications[31].

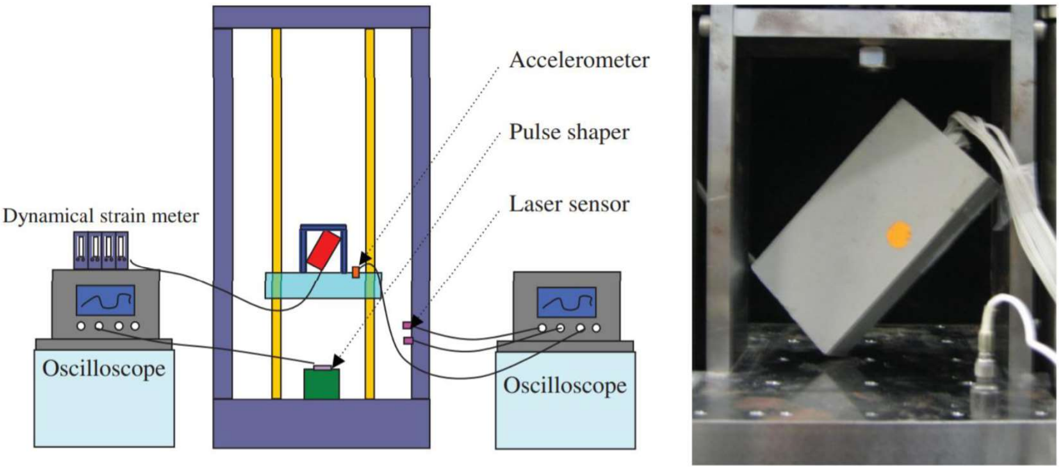

Figure 1-10. Illustration and picture of a drop table[35]

Electrodynamic shakers are readily available and very flexible in terms of simulating different pyroshock loadings (see Figure 1-11). The main advantage is that there is no trial-and-error process in electrodynamic shakers since they have closed-loop control. Desired acceleration levels at required frequencies could be created. However, the main disadvantages of those systems are the limitation of acceleration amplitude and frequency range. Most of the systems could not excite DUT over 3kHz frequencies and over 1000 g's[6]. In other words, electrodynamic shakers are only sufficient to simulate far-field pyroshock loadings.

Metal-to-metal impact test bench, another mechanically-excited pyroshock test system, is mainly based on a resonant structure. A metal impactor is accelerated in different ways and impacted the resonant structure. Then, with the help of resonance, high levels of accelerations are transmitted to DUT. Metal-to-metal impact test system or mechanical impulse pyroshock system (MIPS) is capable of simulation mid-field and far-field pyroshock loads. They are preferred where capacities of electrodynamic shakers are not sufficient.

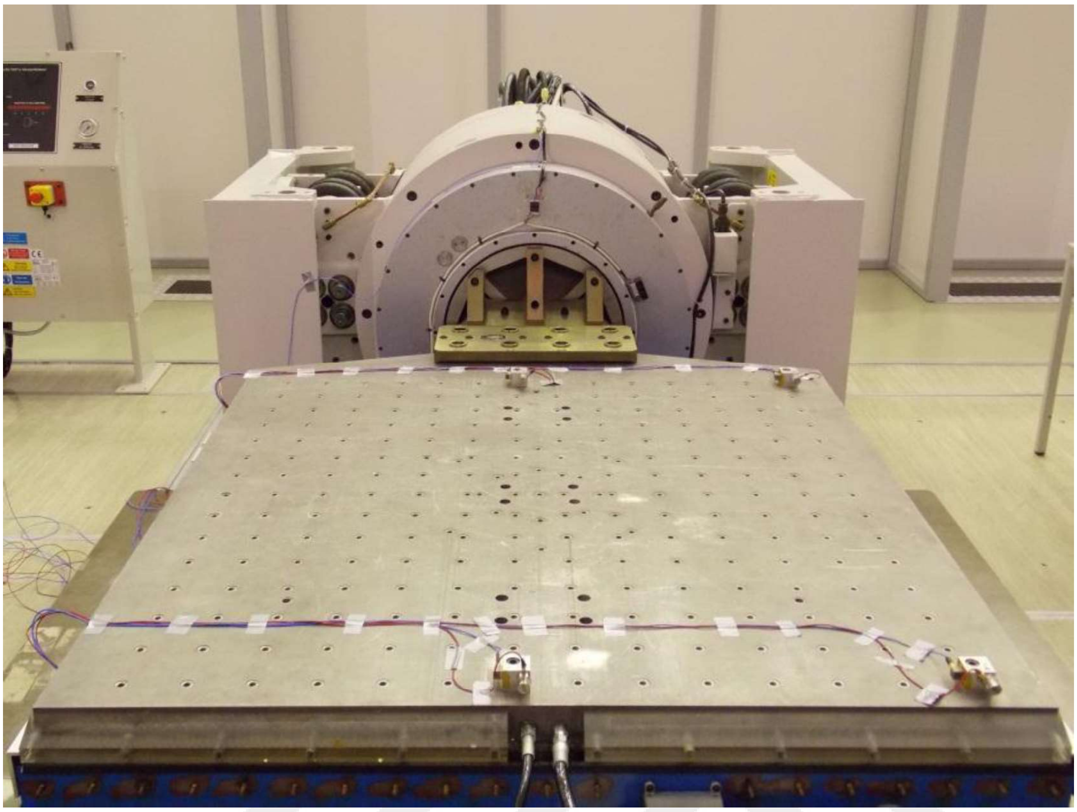

Figure 1-11. Electrodynamic shaker[30]

MIPS systems mainly use a resonant bar, beam, or plate. Some portable devices are studied in literature as well to perform system-level tests, such as the work of Hwang et al. [21]. However, most of the systems are designed for instrument-level tests. All these systems use resonance to amplify and transmit the shock wave and are excited by an impact. In principle, the severity of this impact is adjusted to lead to an elastic shock wave on the structure and does not create any plastic deformation on the test bench. Besides, local plastic deformation at the vicinity of impact, especially systems that simulate mid-field pyroshocks, is inevitable in practice. It is a common application to use another additional plate for the impact area called an anvil plate. It is changed after a certain number of tests and ensures the working life of the test bench by saving the resonant structure to be permanently deformed.

In a resonant bar or Hopkinson's Bar, the first longitudinal resonant frequency of a bar-like structure is used. A schematic illustration and a picture are presented in Figure 1-12. In order not to decrease the level of transmitted acceleration, the resonant bar is hanged so it can vibrate freely with minimum damping. Creating almost free boundary conditions for structure by hanging or placing on top of spring in some cases is preferred for all kinds of resonant structures.

In resonant bar systems, the impactor hits the bar from one end, and DUT is mounted on the other end. It is the most straightforward system to simulate pyroshock, but it has its disadvantages. The resonant bar is designed as the first longitudinal vibration mode that corresponds to the knee frequency of the desired SRS. Thus, it requires different bars for different knee frequencies. Furthermore, the system lack any other tuning parameters as some of the other methods have, such as different impact location, DUT location, mounting additional structures to increase the mass and stiffness, etc. Another possible limitation is the DUT size. As the mounting is for DUT widen, the geometric shape shifts from a rod to a rectangular, and other vibration modes start to contribute significantly to the system's response. As a result, the resonant bar system mainly used for instrument level far and mid-field pyroshock simulations of relatively small structures.

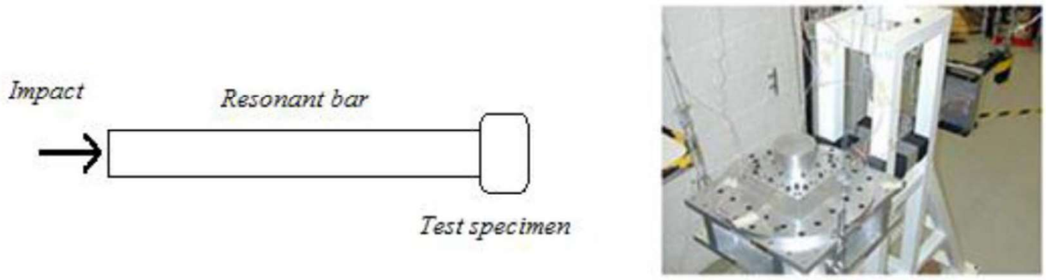

Figure 1-12. Resonant bar[36]

Another method is called the resonant beam method (see Figure 1-13). It is similar to the resonant bar, but the direction of loading is perpendicular to the longitudinal axis of the beam. Thus, it uses bending stress waves instead of longitudinal tension-compression waves to transmit the shock loading. Its main advantage to the resonant bar is that it is possible to tune the knee frequency without changing the shape of the resonant beam. In most resonant beam facilities, there are adjustable clamps on the beam that permits fixing at different positions. Changing the free length of the beam alters the first bending vibration mode so the knee frequency of the SRS of simulated pyroshock.

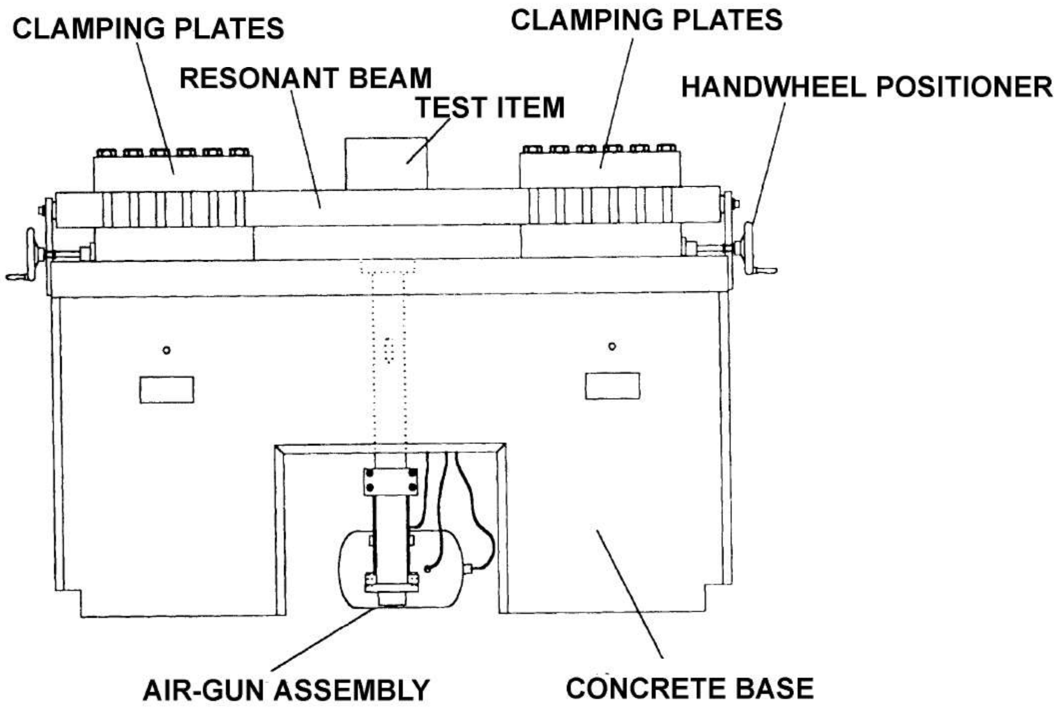

Figure 1-13. Resonant beam [31]

In order to have adjustable clamps, it is preferred to have a table-like structure to mount the resonant beam. Though it has the advantage of changing knee frequency, the adjustable clamping method limits the vibration amplitude and lowers the shock amplitude possible to translate DUT. For mid-field applications where relatively high acceleration levels are required, adjustable clamps limit the usage of those test systems. This limitation could be more severe with the increasing mass of the DUT since a thicker beam is required to provide the desired knee frequency for a heavier DUT. Thus it requires a more violent impact to the beam to transmit the necessary shock. It limits the maximum knee frequency and maximum acceleration levels that could be reached in practical applications due to possible plastic deformation of the test system as the impact becomes more violent. Therefore, it is a preferred method only for instrument level far and mid-field pyroshock simulations of relatively small structures as the resonant bar method.

Another kind of resonant structure, including the one studied in the current work, is the resonant plate. Resonant plate test system, in other words, ringing plate test system, benefits the bending modes of a plate that could be in the shape of a square, rectangle, or triangle – though the last one is infrequent. For almost free boundary conditions, the system is preferred to be hanged by ropes or chains. Other mounting methods are placing on a thick foam or on several springs that permit the structures to vibrate easily (see Figure 1-14).

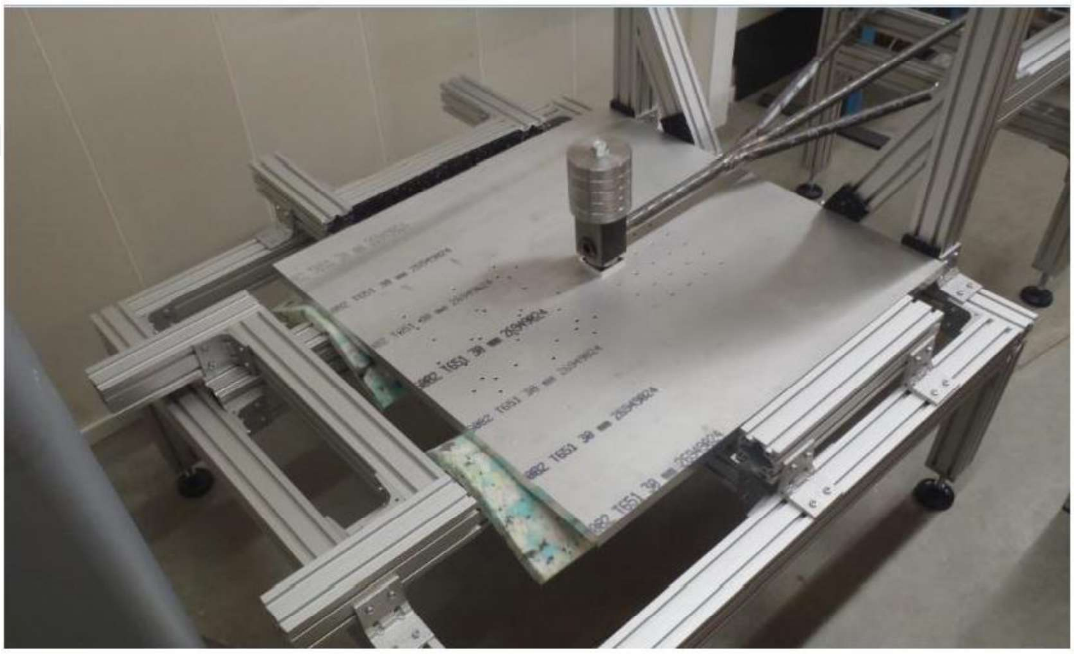

Figure 1-14. Ringing plate [30]

Although they are more complicated and costly, ringing plate test systems have several advantages regarding the resonant beam or bar. Jonsson discussed the design details of a ringing plate pyroshock test system [30]. Impact location and the impact direction could be changed. Most of the systems work in the in-plane (IP) directions and out-of-plane (OOP) direction. In OOP configuration, the impactor could hit different locations on the plate, from up or downside. Impact direction does not change the created shock but is decided according to the application convenience of the impact method and the impactor. Hitting different locations changes the dominant vibration modes excited and create different shock responses throughout the plate. If changing DUT location is also considered, it reveals many different configurations to tune the shock loading. In the IP configuration, the ringing plate is excited from one of the sides and DUT is placed again on top of the plate as in OOP configuration. In this impact configuration, in-plane vibration modes of ringing plate dominate and determine the knee frequency. In order to calibrate shock loading, it is possible to change the position of DUT. However, impact location alternatives are very limited in IP configuration, and most of the time, does not alter the shock considerably. Thus, it is not a parameter to change the impact location in IP configuration; the position is fixed through the structure of the test bench.

Different ringing plate test systems exist in literature in terms of the plate number [37]. The most widely used one is mono-plate but there are systems consisting of two plates mounted on top of each other with or without separators. These systems are called bi-plate. Both of the plates contribute to shock response, and separators provide damping within a particular frequency band.

Metal-to-metal impact test systems use quite different excitation alternatives. Still, two of them are most widely used, a pendulum with a mass attached and a pneumatic gun that uses compressed air to accelerate the projectile. For resonant bar and beam systems, the pneumatic gun is the most preferred method, while any of two could be preferable for the resonant plate test systems. Furthermore, in some systems, two methods exist together to cover both IP and OOP impact configurations.

A pneumatic gun consists of a projectile, a cylindrical pipe, and a compressed air tank with related pneumatic components. The projectile is accelerated with compressed air as a valve opens and lets the air fill the cylinder.

A mass-pendulum system consists of a pendulum system and a mass attached to it, as the name implies. It is simpler than a pneumatic gun but requires a larger space due to the necessary carcass to attach the pendulum. On the other hand, a pneumatic gun needs much less space, and it is a more mobile system, although necessary pneumatic system components such as air tank, valves, hoses, etc.

Metal-to-metal impact test systems widen the pyroshock simulation in shock levels, frequency content, DUT size, and mass limitations without using explosives.

However, they have a significant disadvantage. They are open-loop systems, requiring a trial-and-error process for every shock environment and DUT combination (see, e.g. [24,25,38]). Otherwise, both over-testing and under-testing are possible regarding qualification levels. Discrepancies can occur as the total level of accelerations or local differences in different frequency bands prevent a successful qualification test. Therefore, before testing an instrument or sub-system, a calibration phase is performed with dummy models of DUTs in order to identify the test parameters such as impact velocity, impact, DUT position, etc.

1.2.1.3 Laser Excitation

A new and promising excitation method is laser one. A laser pulse would produce transient localized heating, which would lead to the development of thermo-elastic stresses and strains acting as a source of shock waves [10]. Laser excitation has excellent characteristics up to 1MHz and perfect repeatability, which are valuable for pyroshock simulation compared to more traditional methods, such as MIPS [10]. A typical system consists of a laser generator, mirrors, a focusing lens, and a resonant structure such as a resonant plate. The laser pulse is generated, and it is focused on a particular point on the resonant plate utilizing mirrors and lenses. As the laser hits the plate, it vaporizes some material into plasma form. This plasma creates a tiny explosion and triggers an elastic stress wave on the resonant structure. A schematic of a laser-excited pyroshock simulator is presented in Figure 1-15.

Lee et al. studied a low-energy laser pulse, and only a few g's levels of acceleration could be reached in SRS[39]. However, Yan et al. [22] studied a laser pulse with 1.5 J energy and 15 ns pulse duration and able to reach several thousand g levels. It is concluded that laser excitation could be applicable to mid-field and even for near-field as well. Though laser excitation is a promising method, it is not as mature as other traditional methods such as electrodynamic shaker and metal-to-metal impact systems.

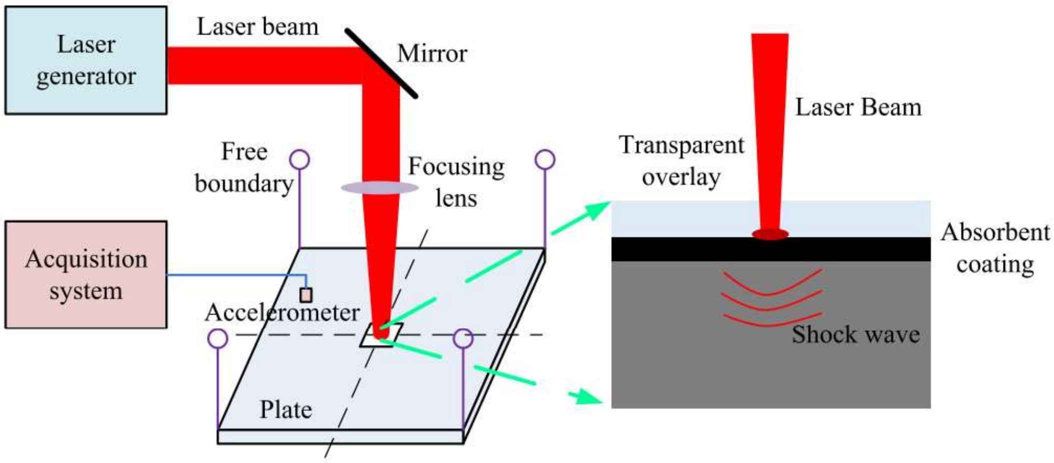

Figure 1-15. Laser shock experiment[22]

1.2.2 Numerical Methods

Numerical analysis techniques have also been employed to test the instrument numerically for desired shock levels or investigate the necessary input parameters to perform an experimental pyroshock simulation with correct shock levels. Although experimental methods remain as the primary pyroshock verification technique, in certain cases they could be replaced with numerical approaches reducing the time and cost substantially. There are two main numerical methods for pyroshock simulation: the finite element method (FEM) and the statistical energy method (SEA). Both of them have their advantages/disadvantages and application regions. For a better prediction performance with numerical methods, hybrids versions are used as well in literature, such as the work of Zhao et al. [40].

1.2.2.1 Finite Element Method

The finite element method is based on the discretization of complex structures into basic shapes and solving the differential equations describing the state of those simple elements. It is a well-known and well-studied method for applications of almost all fields in the interest of engineering. FEM is an approximation method and is known for its accuracy on static and dynamic structural problems. When it comes to the high-frequency dynamic simulation of structures such as pyroshock, several limitations are introduced, and the accuracy of FEM decreases[10]. However, when it is used in these applications with cautions, it could still produce valuable outcomes and estimate the real situation. Therefore, FEM is the most widely used numerical approach for pyroshock simulations(see, e.g. [15,18,24,25,41]). In several studies, including the study of García-Pérez et al.[27] and Siam[28], different approaches for FE analyses of a pyroshock loading are studied. These could be listed as transient analysis, response spectrum analysis, sine transmissibility analysis, and equivalent load analyses[27].

Transient analysis is the most intuitive and the most general approach. It computes the behavior of the structure in the time domain with force or enforced motion applied. Any quantity such as displacements, velocities, accelerations, or stresses could be observed in the time domain. After the necessary property is obtained, it is a straightforward process to create the SRS data to evaluate the pyroshock. The simulation could be done in a direct manner or with modal superposition. Choice of the method depends on the structure and frequency band to be interested. Transient analysis is a computationally expensive method, but this expense is less if the modal transient approach is used. Another limitation needed to be considered is the choice of time step which limits the maximum frequency content of the dynamic transient analysis. For example, if a time step of 0.001s is chosen, the maximum frequency in the analysis will be 1000 Hz. Considering that frequency content up to 10 kHz is necessary for mid-field pyroshock environments, it could bring limitations to assess mid-fields pyroshock environments. It is advised that the time step should be chosen to be small enough that corresponds a frequency of 5 to 10 times greater than the sampling of the shock signal. For a typical mid-field case, the time step should be 0.00001 s. It is not a practically appropriate time step due to computational limitations if implicit time integration is used. Explicit time integration is an effective alternative to overcome this problem, as preferred in this thesis study.

The response spectrum method is a frequency-based computational approach. It depends on the calculation of normal modes of structure, and an SRS graph is given as input. Then the summation of modes with the different methods is calculated to obtain the response of the structure to the given SRS. Several different summation methods are introduced: ABS method, which considers that every modal peak values occur at the same time and phase and sums all of them, SRSS (The Squared Root of the Summation of Squared Values) method, which assumes different modal peaks occur at different times and phases. The response spectrum method results vary substantially according to the chosen summation rule, so it is necessary to correlate with test results beforehand any application. It is the main disadvantage of this method.

Another method is the sine transmissibility analysis. It is based on the frequency response analysis of the structure. The transfer function is extracted for selected nodes and multiplied with a factor to find the sine transmissibility. Then input SRS is multiplied with sine transmissibility to find the output SRS of selected nodes. It is a computationally inexpensive method, but it is not accurate in terms of the peak acceleration values due to the damping difference between the real structure and the simulation model. Most of the time, relatively low damping is used for the simulation method, and unphysical peaks are observed.

The last method, equivalent load analysis, is the simplest method among all. It consists of static analysis with a static-equivalent load of the real dynamic case. It is fast and robust if an accurate equivalent force is found. There is no standard, but different formulas for the equivalent load, and the application ranges of these formulas are limited to specific cases.

1.2.2.2 Statistical Energy Analysis

Statistical Energy Analysis (SEA) method is one of the main approaches in the literature for pyroshock simulations (see, e.g. [42-43]). Contrary to FEM, SEA is not a deterministic but statistical method based on energy balances. It is useful for high-frequency region. It solves a power balance that consist of power leaving the system, entering the system and dissipated by the system. This concept could be applied to sub-systems, where these subsystems represent similar vibration modes or vibration modes in a specific frequency range for pyroshock application. It is not one of the few but the only alternative to handle the dynamic response of the structure for high frequencies. However, the method has several disadvantages. All subsystems and energy flow paths between those subsystems are constructed manually, leads to different results for different constructions. Another disadvantage is that it is valid only for high frequencies, and it fails at low frequencies. Lastly, it is not a method to find the absolute values for most cases but to examine the trends only [10].

1.2.2.3 Hybrid Method

For a better prediction performance for numerical methods, their hybrid versions could be employed as well. Among such studies (see e.g., [40, 44-46]), the work of Zhao et al. distinguishes as it exemplifies a successful application of a hybrid method [40].

Combining two powerful methods, FEM and SEA, leads to a robust solution for both low and high-frequency ranges. Zhao applied the FEM-SEA hybrid method to a typical L-shaped part used in aerospace structures. Legs of the L-shaped design, sandwich cabin boards, are modeled with SEA, and the connection beam between them is modeled with FEM (Figure 1-16). Then numerical results of this hybrid model are compared with experimental results. The performance of the hybrid model for a pyroshock application that contains a wide frequency range is promising.

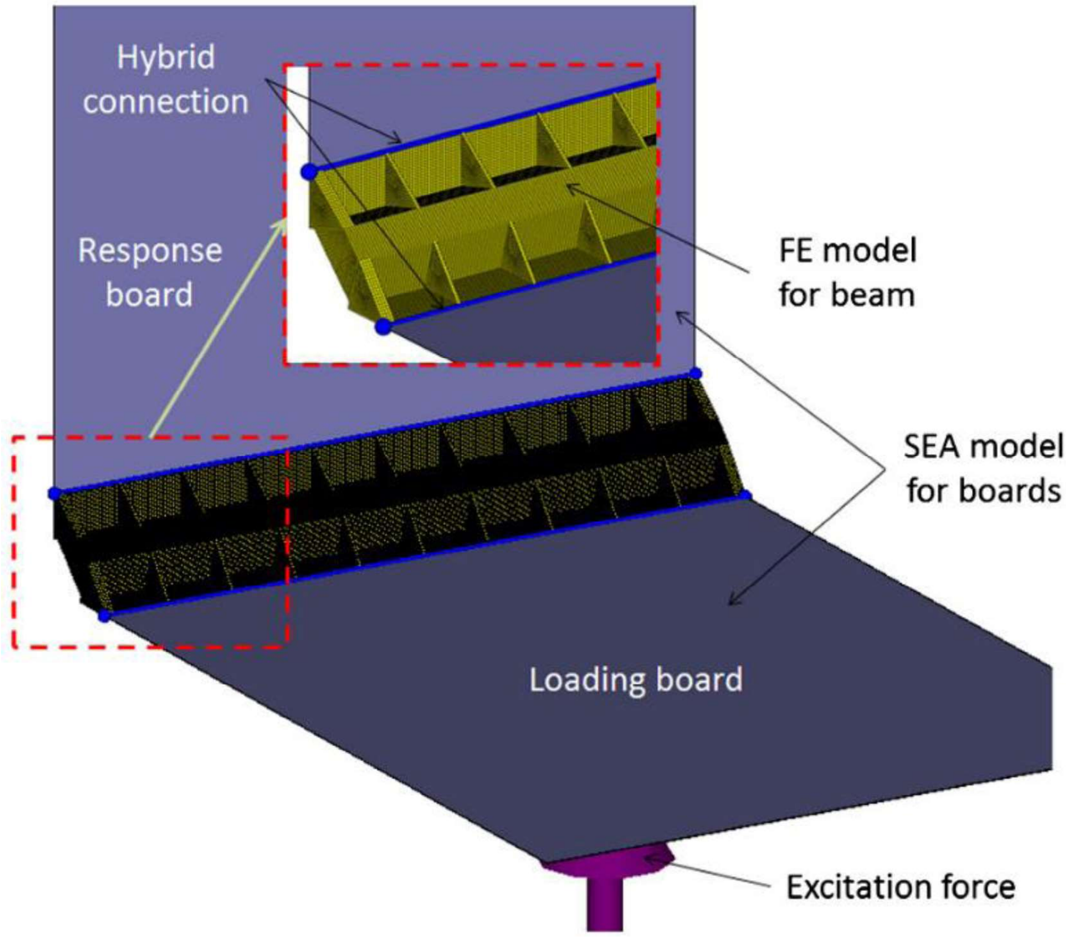

Figure 1-16. FE-SEA hybrid model of an L-shaped structure [40]

1.3 Scope of the Thesis

In this thesis, experimental and numerical pyroshock test results of a metal-to-metal impact based ringing plate test system which can mimic far-field and mid-field pyroshock applications are presented with a focus on a correlation process of experimental results with explicit FE simulations. Furthermore, it is exemplified that FE simulations promise to shorten the trial-and-error phase of any metal-to-metal impact open-loop pyroshock test system in terms of shifting some of the trials with explicit FEM instead of performing on the ringing plate test bench.

In order to perform experimental studies, a ringing plate test system is designed. A pneumatic gun is utilized as the test bench's excitation method and design parameters are specified according to project goals with the contributions of preliminary explicit FE analyses. The design process is summarized shortly, as well as detailed results of those FE simulations.

Several experiments are performed with the designed ringing plate test system where the effect of different configurations such as the speed of projectile and measurement location is considered. In the experiments, the speed of the projectile in the pneumatic excitation system and the acceleration from different locations are measured. The former is used as an input for the numerical simulations, while the latter is converted to SRS curves and compared with the results of FE simulations. The correlation process and the influence of different simulation parameters are discussed in detail as well as the performance of the explicit FE method in predicting SRS curves within various frequency ranges and acceleration levels. It is showed that even though Lee et al. mentioned that FE simulations are considered to have low accuracy for pyroshock problems [10], their accuracy could be substantially increased with a correct set of simulation parameters. Furthermore, a pyroshock test with a dummy instrument mounted on the system is considered as a case study. The FE simulations' performance is evaluated to create an alternative for trial-and-error phases of ringing plate pyroshock test systems. Overall, the thesis work presents a unique study combining both experiments and explicit FE simulations on a ringing plate test system.

The thesis is organized as follows. The summarized design process and preliminary FE simulations are presented in Chapter 2. The experiments with the designed system are presented in Chapter 3. FE model details, SRS results and the comparison of numerical and experimental studies with an insight of correlation process are discussed in this chapter. A case study for a pyroshock test with a dummy instrument that exemplifies the explicit FE method's potential for the trial-and-error phase is presented in Chapter 4. Lastly, conclusions are summarized in Chapter 5.

CHAPTER 2

PYROSHOCK TEST BENCH DESIGN

2.1 Project Aims and Conceptual Design

The main functionality of a pyroshock test bench can be stated as "qualifying the structure under desired pyroshock loading by exposing that structure to required shock environment." Therefore, pyroshock test benches are used when testing the entire system with real pyrotechnic devices is not possible. Instead, pyroshock test benches somehow "simulate" the necessary shock environment.

It is convenient for a systematic design process to decompose the mentioned primary function into sub-functions and search for the best solutions. However, it is essential to define the goals as the first step to that systematic design process. Pyrohock test system used for experimental studies in this thesis work is funded by The Scientific and Technological Research Council of Turkey through project number 3170878. Thus, the project implies a particular set of requirements and goals. These can be summarized as follows:

- Test system should be capable of simulating both far-field and mid-field pyroshock environments.
- Test system should be capable of testing instruments with dimensions up to 500mm*500mm*500mm and mass up to 15kg.
- Test system should be mobile and fit in a volume of 5m*5m*2m.
- No special security permissions should be necessary.

The primary function of the test system can be divided into three sub-functions regarding the project goals:

1. Transmitting shock loading to DUT
2. Exciting the system to create shock environment

3. Support the structure of the test system

The goals of the project impose several initial constraints to design alternatives. Electrodynamic shakers are not an option since they are not capable of simulating mid-filed pyroshocks. Using pyrotechnics is not an option as well, considering necessary special permissions and safety certificates. That leaves the MIPS are the only option. Even in the category of MIPS, several solutions could be evaluated for every sub-function. Cross-choices between those alternatives conclude tens of different test system configuration. Various possible solutions for sub-functions are summarized in Table 2.1.

Table 2.1 Solution alternatives for sub-functions

Sub-Function 1: Transmitting shock loading to DUT	Sub-Function 2: Exciting the system to create shock loading	Sub-Function 3: Carcass to support the structure of the test system
Resonant Bar Resonant Beam Tunable Resonant Beam Resonant Plate Resonant Bi-Plate	Drop Hammer Pendulum Hammer Pneumatic Piston Pneumatic Gun Combination Hammers	Resting on Foam Pad Hanged by Ropes Resting on Springs Clamped

With the DUT size requirement, it is evident that the required resonant structure sizes are too bulky to handle in terms of reaching mid-field pyroshock accelerations levels, i.e., level in the range of 1000g-10000g for the resonant bar or beam solutions. Those acceleration levels are theoretically reachable on a beam with a 500mm*500mm cross-section if enough energy is transmitted to the resonant structure. However, a metal-to-metal impact that creates thousands of g's on such a design is very likely to develop permanent deformation on the test bench. That substantially reduces the life the test bench and requires changing of the resonant structure frequently, which is not an acceptable solution. Therefore, it leaves the option of resonant plates for sub-function 1. It is convenient to start with a mono-plate and upgrade it to a bi-plate if required after the initial prototype results.

For sub-function 2, hammers and pneumatic systems are both flexible in terms of the mass that impact the resonant structure. However, considering severe impacts may be necessary to reach mid-field pyroshock accelerations levels with a 15 kg DUT, pneumatic systems are more flexible and feasible to reach high impact speeds than hammer systems. The impact speed of hammers is dependent on pendulum length or drop height. That cause large carcass structures with increasing impact speed requirements that possibly conflict with test system dimension limitations proposed above. It concludes that the pneumatic options for the second sub-function even it is much harder to control impact speed and provide repeatability on those systems comparing to hammer systems. The pneumatic gun is the chosen one since more examples in the literature exist.

Within different carcass structure alternatives, resting on springs gives the best combination of mobility and almost-free boundary conditions to prevent excessive damping of the vibrations of the resonant structure. Therefore, the concluded conceptual design is a resonant bi-plate or mono-plate resting on springs and excitation with a pneumatic gun as given in Table 2.2.

Table 2.2 Decided conceptual design

Sub-Function 1: Transmitting shock loading to DUT	Sub-Function 2: Exciting the system to create shock loading	Sub-Function 3: Carcass to support the structure of the test system
Resonant Plate	Pneumatic Gun	Resting on Springs

2.2 Design Parameters Sensitivity Simulations

Resonant structure and excitation mechanism together specify the characteristics of shock environments that could be simulated in terms of knee frequency and acceleration levels. Therefore, a set of simulations is performed to decide the design parameters of the resonant plate and the pneumatic gun. Those preliminary simulations are not high-fidelity but could represent the effect of different parameters on the output SRS in a comparative manner. They are valuable to understand the effect of various design parameters beforehand of critical design.

Simulations are performed with explicit FE method via a commercial code, LSTC Ls-Dyna. Simulations here are performed with default parameters, and the FE model consists of a resonant plate, a typical DUT, and the impactor (Figure 2-1). Details of FE modeling and discussion of used parameters and approaches are presented in Section 3.2 and are not mentioned here to avoid repetition. This section focuses on the result of preliminary simulations and discusses them in the context of the design phase. In order to isolate the effect of a parameter, analysis sets are performed only by changing that parameter but keeping the rest of the parameters constant.

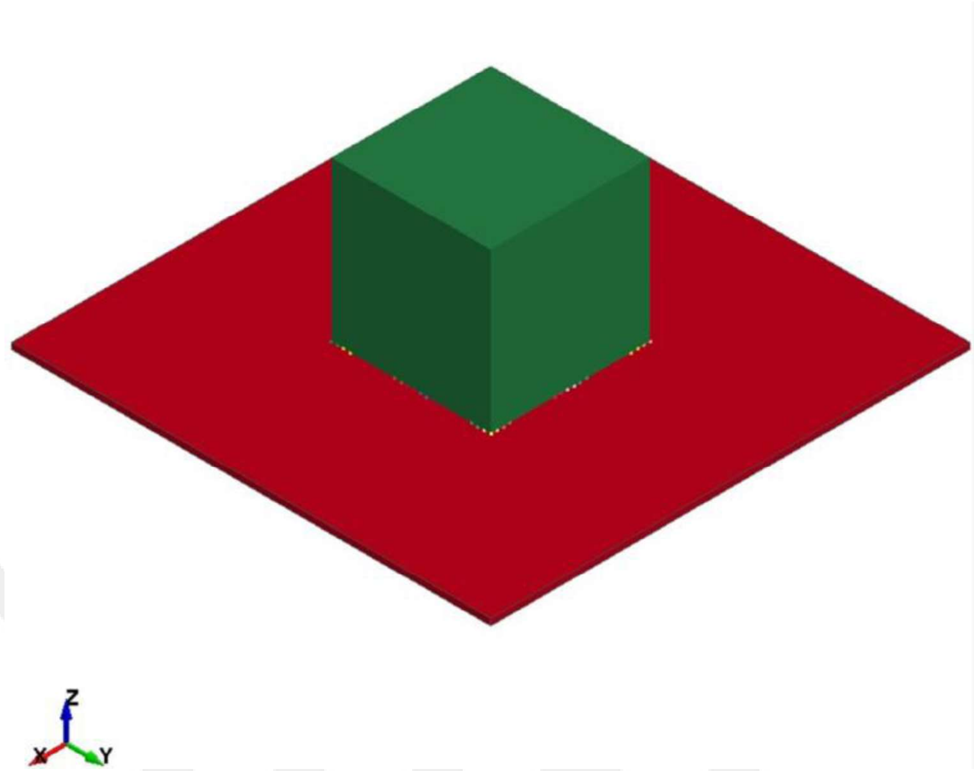

(a)

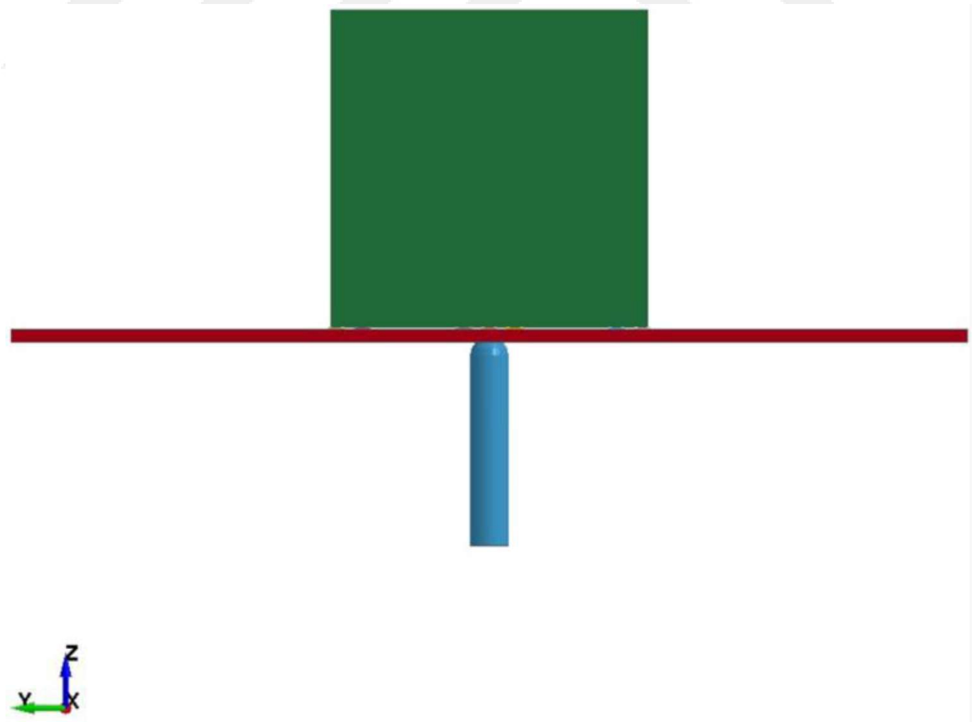

(b)

Figure 2-1. Preliminary FE Model. (a) Isometric View (b) Front View

2.2.1 Impact Velocity

Increasing impact velocity increases the amplitude of SRS throughout the whole frequency range, but the curve's trend remains constant. In a log-log scale of SRS, it seems that increasing impact speed lifts the curve as keeping the shape exactly (see Figure 2-2). Impact speed is one of the primary adjustment parameters to tune the shock environment simulated.

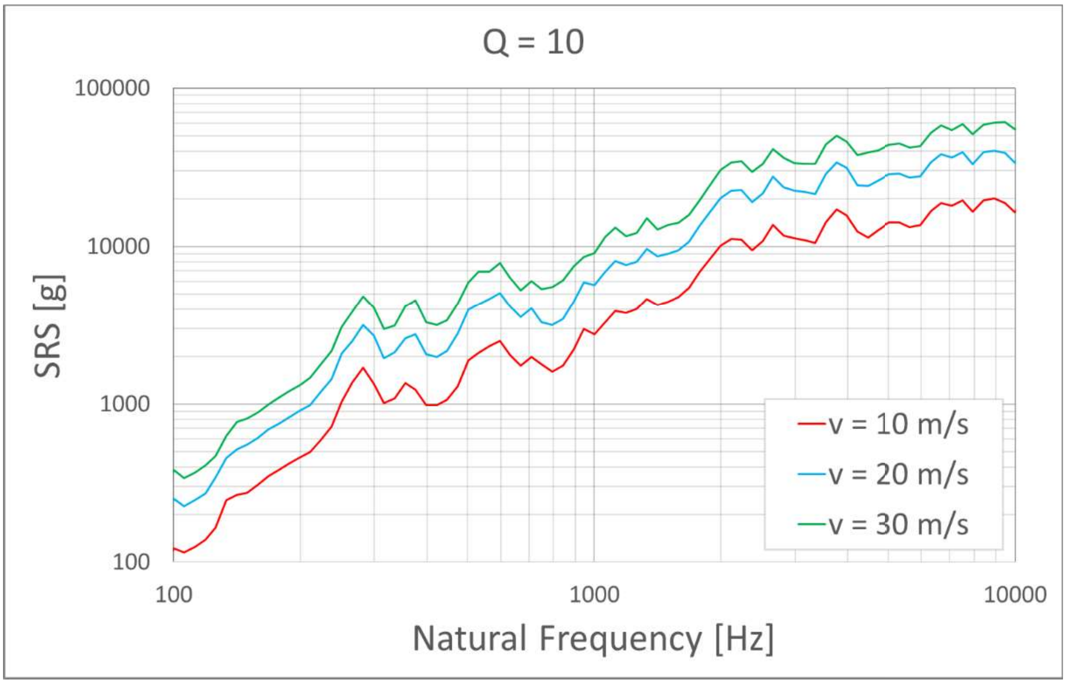

Figure 2-2. Impact speed effect

2.2.2 Impactor Mass

Impactors that have the same shape at the impact region but have 4-10-15 kg masses are simulated. The effect of impactor mass is not as significant as impact speed. It affects the low frequencies substantially and has an almost negligible impact on the higher frequency band. The amplitude of lower frequencies increases as impactor mass increases (see Figure 2-3). It is concluded that impactor mass changes the SRS slope before knee frequency and could be used as a tuning parameter.

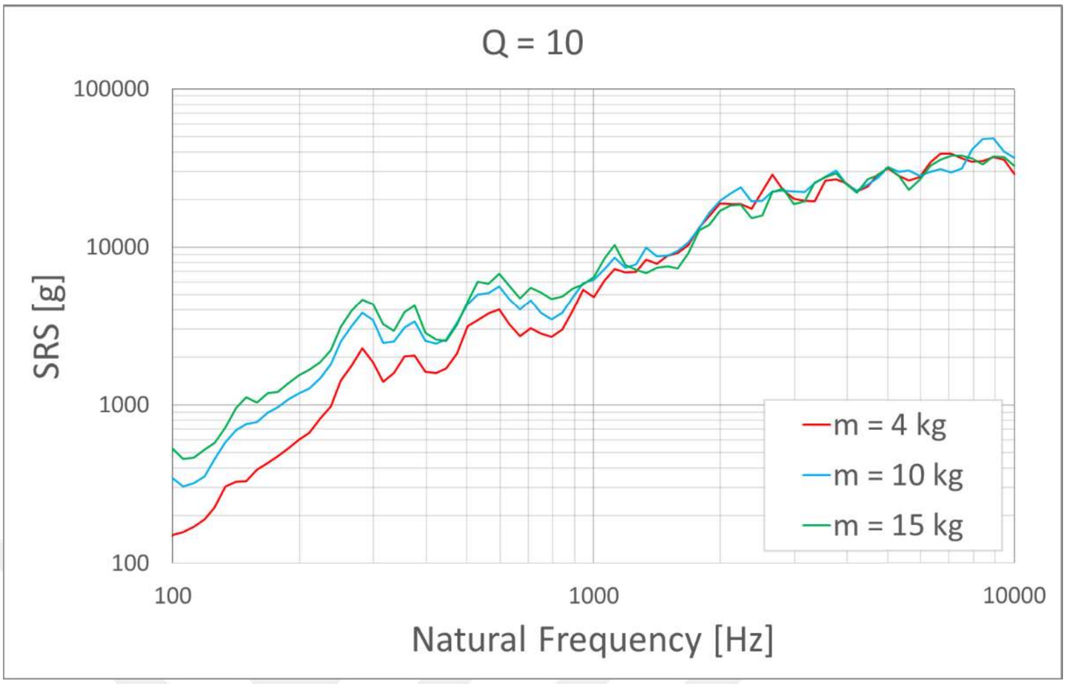

Figure 2-3. Impactor mass effect

Increasing the mass and increasing the velocity of the projectile both increase the impact energy. It was expected that if the energy increases same amount by means of projectile mass or velocity, SRS amplitude increases the same amount. However, Figure 2-2 and Figure 2-3 shows that the rise are not same. It could be explained with the difference of excitation for different frequency ranges. Increasing mass scales up the impact duration and the excitation of relatively low frequencies while damps the higher frequencies. On the contrary, increasing the velocity raises the excitation throughout the all frequency range.

2.2.3 The shape of Contact Region of Impactor

The shape of the impactor's contact surface is changed by lowering the angle on the tip of the impactor geometry. It decreases the flat surface at the contact region of the impactor. Different geometries that have flat surfaces with 30-45-60mm radiuses are analyzed (see Figure 2-4).

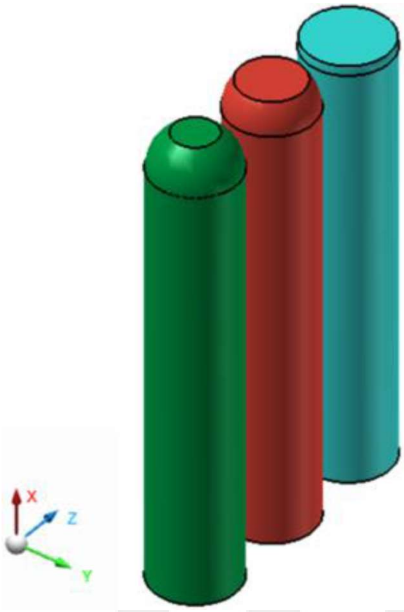

Figure 2-4. Impactors with different contact surfaces

There is almost no difference in the low and mid-frequency bands on SRS for different contact surfaces (see Figure 2-5). As the contact surface becomes smaller, the amplitude decreases in the high-frequency band. However, the drop amount is subtle, and the contact surface is relatively ineffective to be beneficial as a tuning parameter.

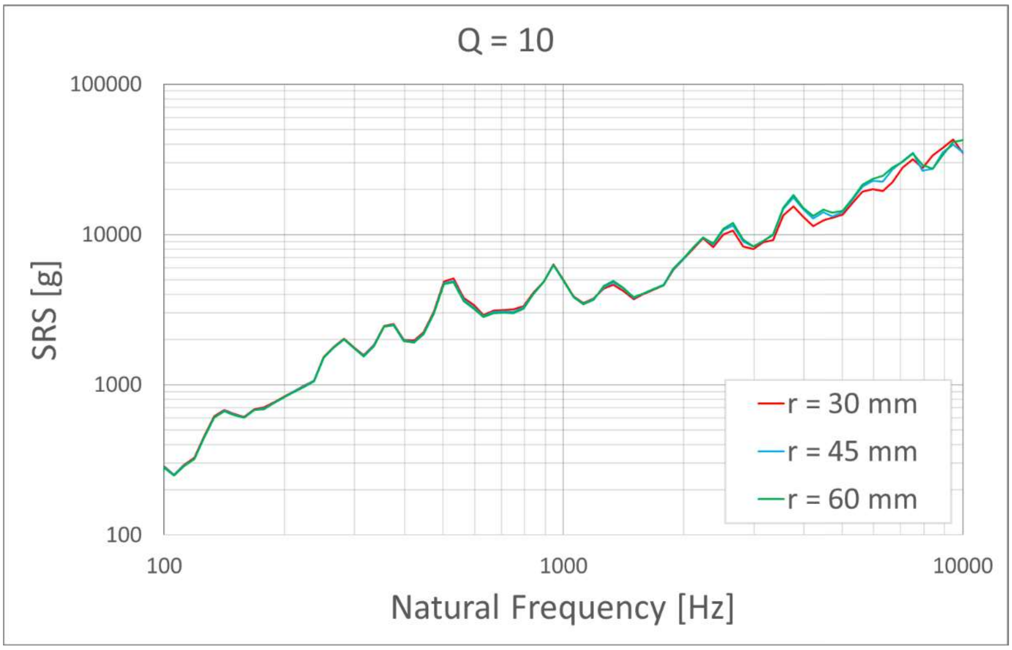

Figure 2-5. Effect of the contact region of the impactor

2.2.4 Resonant Plate Material

Aluminum and steel resonant plates are compared as they are the most common material alternatives.

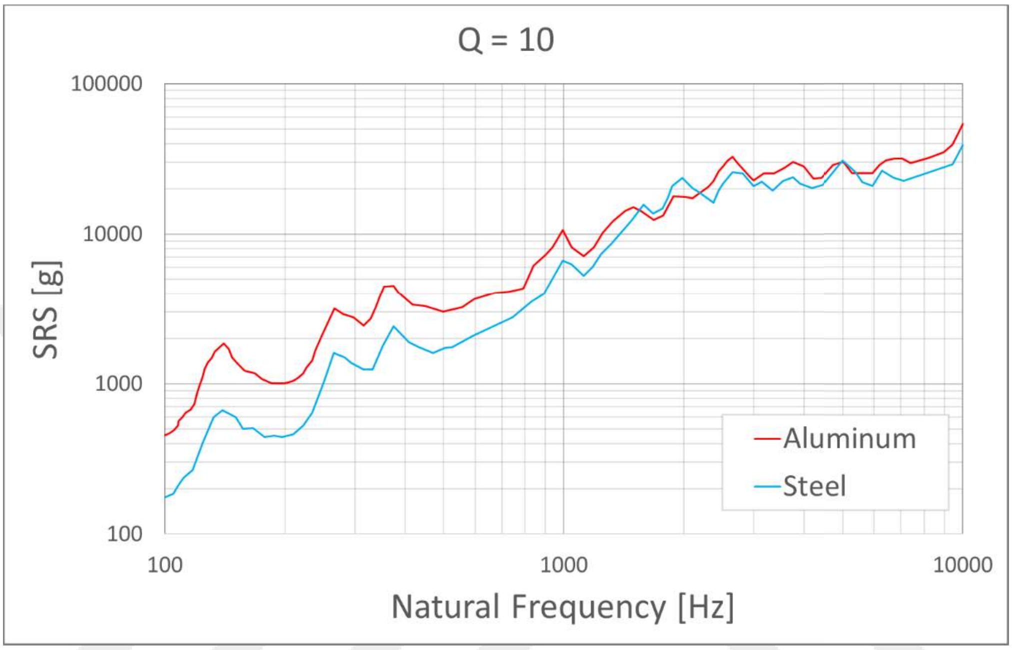

Figure 2-6. Effect of the resonant plate material

Figure 2-6 shows that the amplitude of SRS is higher on the aluminum resonant plate, although it does not increase equally for all frequency bands when examined on a log-log scale. Lower frequencies tend to raise more. Another significant effect is the change in knee frequency. The aluminum resonant plate has a higher knee frequency as expected due to a decrease in the mass of the plate.

2.2.5 Resonant Plate Thickness

The main effect of an increase in the resonant plate thickness is the induced increase in the bending stiffness, which substantially affects the resonance frequencies of bending vibration modes. Considering the main working principle of resonant plate based on bending resonances, it is understandable that changing thickness influences the whole SRS curve as presented in Figure 2-7 for 10-20-30mm thickness of the plate.

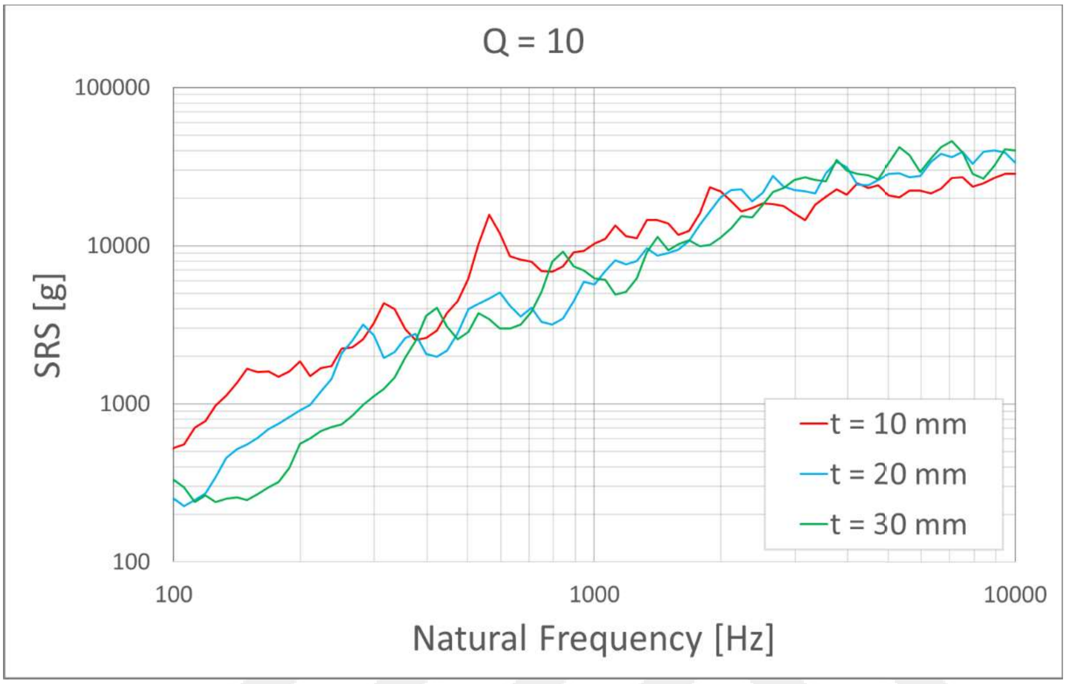

Figure 2-7. Resonant late thickness effect

Changes on all frequency bands are chaotic, as seen in Figure 2-7. However, several outcomes can be extracted from the simulation results. Increasing thickness increases the knee frequency as expected since a thicker plate has a higher fundamental bending vibration frequency. Another observation is the amplitude of lower frequencies decreases, whereas the amplitude of higher frequencies increases with increasing thickness. It is one of the most influential parameters for designing the pyroshock system together with the impactor mass and impact speed range of the system.

2.3 Final Design

The final design is based on the results of conceptual design and preliminary FE simulations. Results of preliminary simulations represents the effect of the different design parameters for the capability of simulating different pyroshock environments of the test bench. Regarding main design parameters analyzed and presented previous sections, it is clear that performance of the system is up to resonant plate and pneumatic gun, which specifies the impact velocity and the impactor mass. Final design for experimental system is shaped considering the results of preliminary simulations.

However, there are still several uncertainties at this phase, which are addressed by choosing the option assumed to provide more flexibility on the test system to simulate different shock environments. Firstly, the detailed design of the most important two components, namely the resonant plate and the pneumatic gun, are completed according to goals. Then a carcass is designed, and appropriate springs are chosen for the resonant plate. Later on, necessary pneumatic components are selected regarding designed impactors and estimated impact speeds. As mentioned in the introduction chapter, the focus of this thesis work is on explicit FE analyses. Thus the author prefer to give only a summary of the final design in this section

2.3.1 Resonant Plate and Support Structure

The resonant plate is sized as a square 1500mm*1500mm plate with a constant thickness of 25mm. It is manufactured from Al 7075 due to the very low damping characteristic of Aluminum 7XXX series. It increases acceleration levels that could be transferred to DUT. 225 holes are drilled, with an equal distance of 50mm between them, at the middle 750mm*750mm region of the plate to ensure different mount positions for DUTs are possible. A 3D CAD model representation of the resonant plate is shown in Figure 2-8.

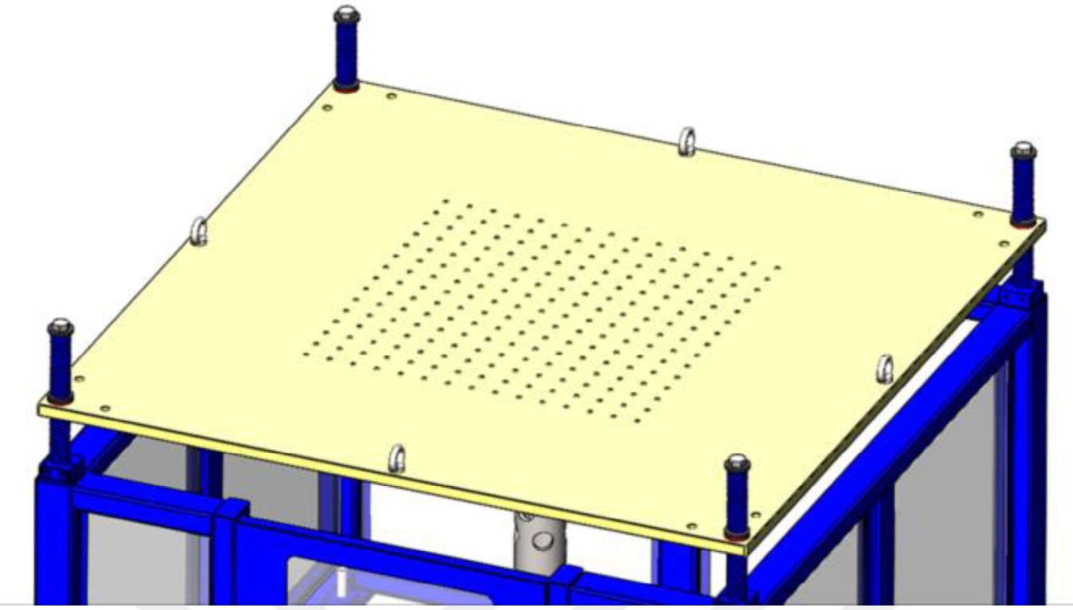
Figure 2-8. Resonant Plate

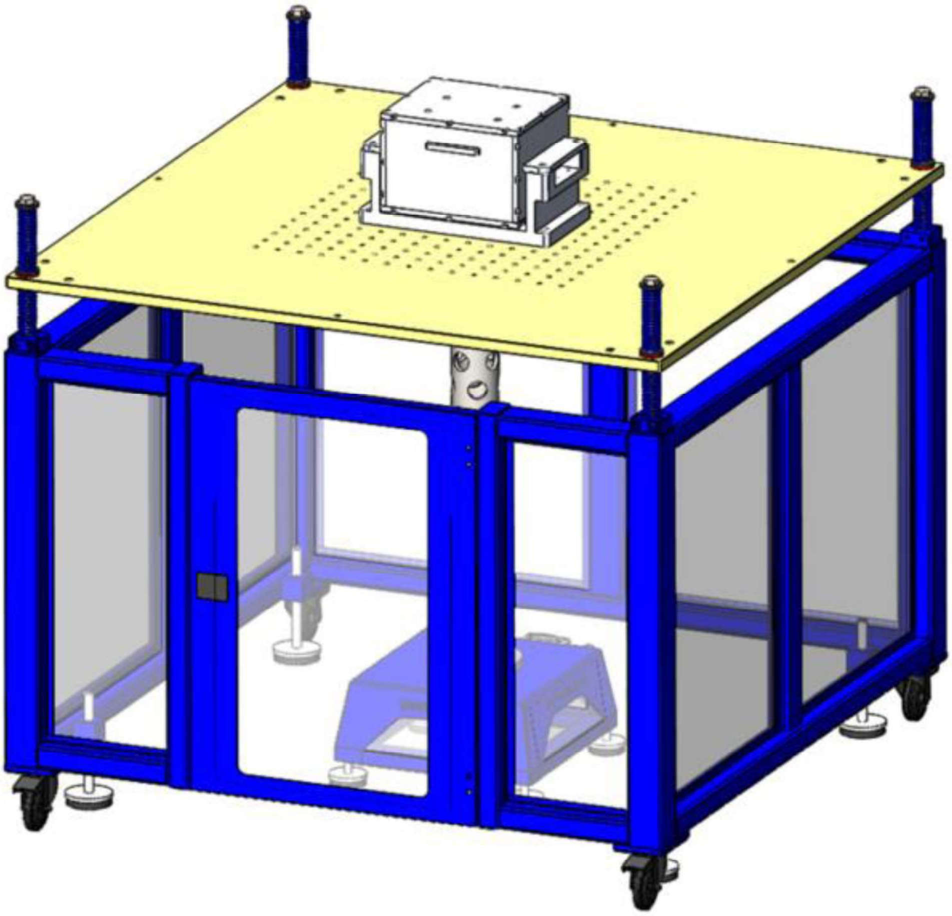
Figure 2-9. Resonant plate with support structure

Resonant plate mounted on a support structure made from steel via M20 bolts from corners. In order to provide almost free boundary conditions, the resonant plate is supported by springs from top and bottom with bushings at the middle. The resonant plate can slide in the vertical axis on M20 bolts, and excessive displacement is prevented by spring. A carcass from aluminum profiles is manufactured to position the resonant plate at a certain height from the ground to have enough space for the pneumatic gun.

2.3.2 Pneumatic System

The system is excited with a 10kg impactor. The impactor is accelerated through a pneumatic gun. The whole pneumatic system consists of an impactor, a pneumatic gun, an air tank, several valves, and a hose (see Figure 2-10). The air tank provides ready-to-use pressurized air. As the valve opens at the output of the air tank, the pressurized air goes through the hose and it starts to exerts a force on the flat lower surface of the projectile. The projectile starts to accelerate and moves upwards. As it passes the holes on the gun and it hits the anvil plate, the pressurized air drains off and the projectile comes back to rest after the impact.

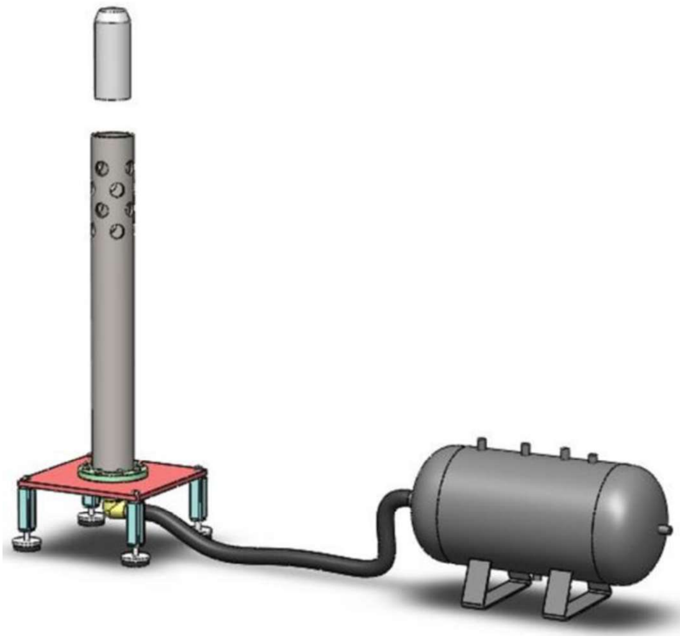

Figure 2-10. Pneumatic System

The system is designed to withstand 10 bar pressure even though the pneumatic system's maximum working pressure is planned to be 6 bar. A PLC system controls valves that regulate the air and controls the speed of the projectile.

2.3.3 Assembly

The whole assembly of the ringing plate test system comprises a square resonant plate positioned horizontally on springs, a stationary pneumatic gun, a pressurized air tank, and a PCL control system shown in Figure 2-11. The pneumatic gun is placed under the resonant plate and aligned at the center point. There is no direct mechanical connection between the gun and the resonant plate to eliminate any possible force and acceleration transmission to the plate. The desired pyroshock environment is obtained with the impact between the resonant plate and the pneumatically accelerated projectile. The collision occurs under the resonant plate, where an anvil plate is placed to prevent local plastic deformation.

Figure 2-11. Assembly of the ringing plate pyroshock test system

As a natural outcome of the current design, the system works only in the vertical direction. The DUT is mounted at the resonant plate's top surface aligned with the center or any other position depending on the pyroshock environment requirements. In order to conduct experiments in different directions, the instrument should be rotated and needs to be fixed to the plate with an L or U-shaped adaptor plate.

A particular pyroshock environment is obtained through different tuning parameters, including the thickness and material of the anvil plate, the velocity and weight of the impactor, the instrument's position, the thickness, size, and material of the instrument adaptor plate. Like other MIPS test systems in literature, it is an open-loop system that requires a calibration phase to ensure whether the necessary pyroshock loading is applied to DUT. Thus, a representative dummy model of the instrument is used for the calibration process to prevent possible damage to the real device.

CHAPTER 3

EXPERIMENTAL AND NUMERICAL PYROSHOCK SIMULATIONS WITH RINGING PLATE TEST SYSTEM

3.1 Experimental Pyroshock Simulations

The experiments presented in this section are done without any DUT. The primary purpose of performing tests directly on the resonant plate is to generate experimental pyroshock data to be used for the development of correlated explicit FE models. The experiments are performed using the ringing plate test bench described in the previous chapter. However, in order to decrease the complexity of the system anvil plate is not used in the experiments of this section.

Two sets of experiments are performed in order to create the necessary experimental data. In the first set, the velocity of the impactor is measured just before the collision with the resonant plate. The pressure of the pneumatic system can be tuned as a parameter that would lead to the adjustment of the impact velocity, and as a direct outcome the amplitude of the pyroshock. However, since the pneumatic system is not modeled in FE procedure, for the sake of simplicity, it creates an essential need to know the velocity of the projectile in order to give it as an initial condition for all FE simulations. Therefore, the velocity of the projectile is measured by two laser sensors that are placed in the same vertical direction aligned with the pneumatic gun and positioned as close as possible to the collision point with a distance of 35mm between them as shown in Figure 3-1. The signals from both sensors are gathered and evaluated by considering the time lag between signals and the physical distance of sensors. A sample signal data is presented in Figure 3-2.

Figure 3-1. Laser sensors for velocity measurement

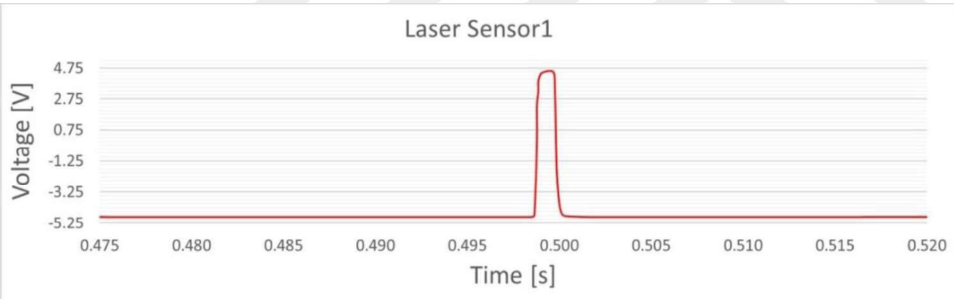

(a) Lower laser sensor

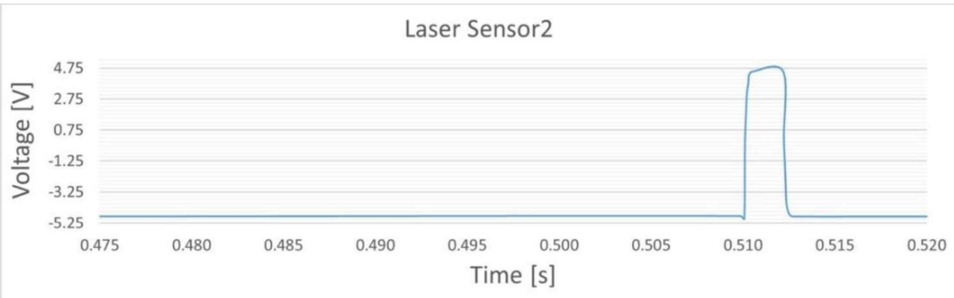

(b) Upper laser sensor

Figure 3-2. Sample signal data from laser sensors. (a) Upper laser sensor and (b) Lower laser sensor

A total of 8 tests are performed with various pressures. In order to check the consistency of the pneumatic system and the PLC control unit, every pressure is tested twice and the velocity values are compared. Certain scatter occurs in the results and it is in a reasonable range, and the system shows consistency to obtain the same velocity for the same pressure values as shown in Table 3.1.

Table 3.1 Velocity Test Results

Test No	Mass of Impactor [kg]	Pressure [bar]	Measured Velocity [m/s]
01	10	0.46	3.07
02	10	0.46	3.10
03	10	0.88	5.83
04	10	0.88	5.74
05	10	1.60	8.75
06	10	1.60	8.97
07	10	2.80	12.07
08	10	2.80	11.67

The second set of experiments is performed to gather the necessary acceleration-time data for correlation and calibration of FE models. A piezo-resistive type of single-axis shock accelerometer is placed on the resonant plate with a simple rectangular adaptor plate and 4xM8 steel bolts. Acceleration – time data are recorded for six different scenarios with three different velocities on two different locations, as presented in Figure 3-3. Anvil plate is removed to make the system simpler to identify the effect of different parameters in FE simulations. As a result of this, even though the system is capable of testing the mid-frequency pyroshocks and works with pressure up to 6 bar, the pressure is limited to 1.20 bar and stayed within the level of far-field pyroshock to ensure the resonant plate do not undergo plastic deformations. Test conditions are illustrated in Table 3.2.

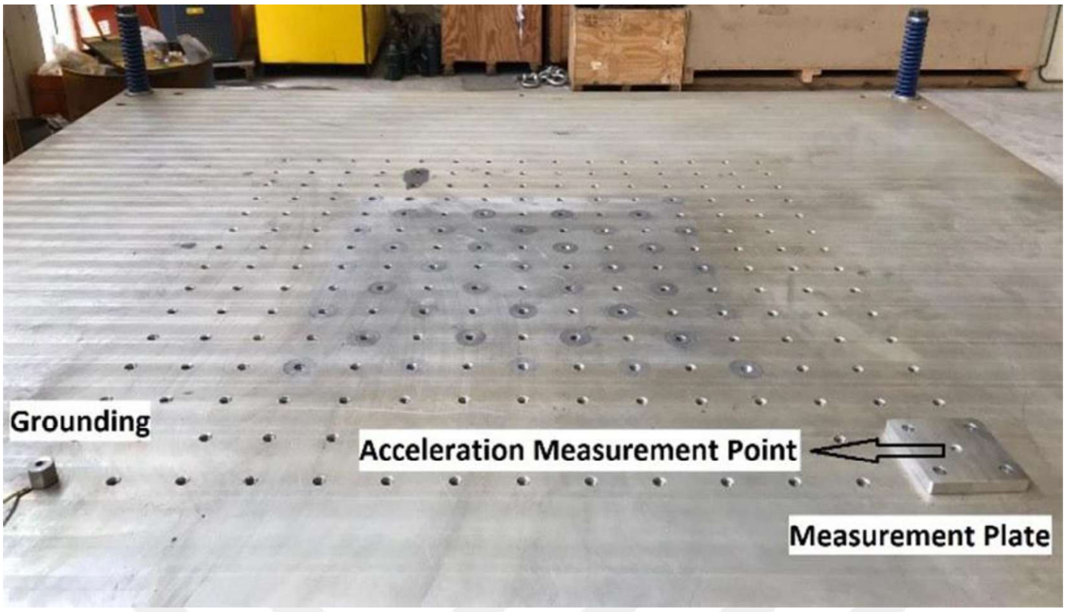

(a) Position of Loc1

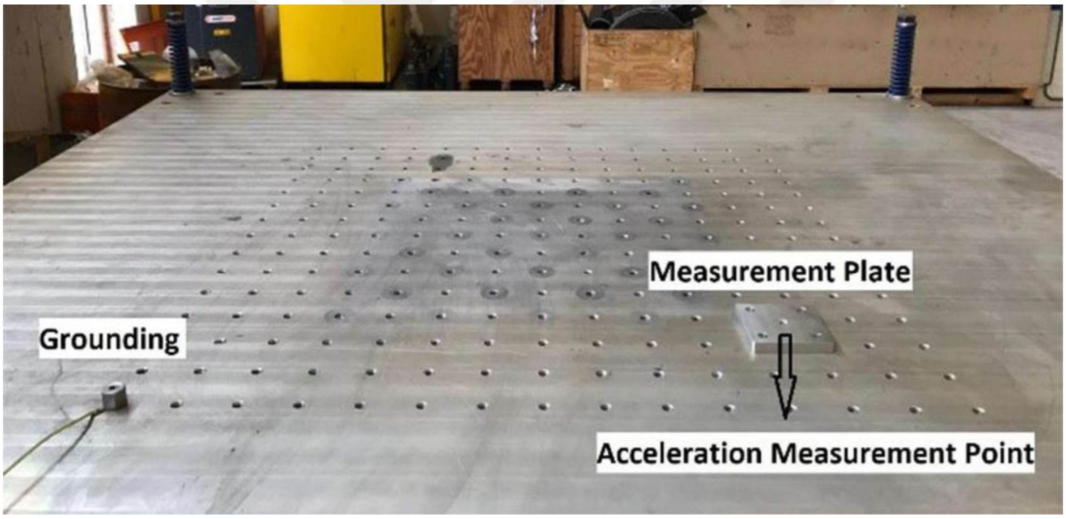

(b) Position of Loc2

Figure 3-3. Illustration of the locations. (a) Position of Loc1 (b) Position of Loc2

A total of 18 tests are performed. Acceleration - time data is collected with 1MHz sampling rate, and it is converted to Shock Response Spectrum (SRS) curves and evaluated in this form due to the difficulty of interpretation of transient acceleration data for pyroshock loading owing to its chaotic nature. The test system is designed to simulate mid-field and far-field pyroshocks, thus it is reasonable to analyze SRS curves within a frequency range between 100 Hz to 10 kHz [10].

Table 3.2 Conditions of test scenarios

Scenario No	Pressure [bar]	Location
01	0.60	Loc1
02	0.90	Loc1
03	1.20	Loc1
04	0.60	Loc2
05	0.90	Loc2
06	1.20	Loc2

In order to ensure the repeatability of the shocks, it is imposed that 3 successive tests with the same test parameters create a shock response spectrum curve for the measured out-of-plane acceleration within +/- 1dB tolerance band throughout the whole frequency range. It is observed that the system has desired repeatability in general according to the SRS curves presented in Figure 3-4. However, Scenario 06 is an exception, where 2 successive tests agree with each other while the third one is far from agreement with an unrealistic SRS curve. Thus, the third case for Scenario 06 is disregarded for FE simulation-experiment correlation study. A detailed survey on the accelerometer after that test reveals that it is short-circuited and does not give the correct acceleration results for that very last test. This situation shows the importance of the repeatability check of SRS curves once again. Apart from the 3rd test of Scenario 06, small deviations occur for one of the third tests of both Scenario 02 and 05 in the range of 7 kHz – 10 kHz but they are still in the tolerance band. Those aspects are taking into consideration for correlation work presented in the following sections.

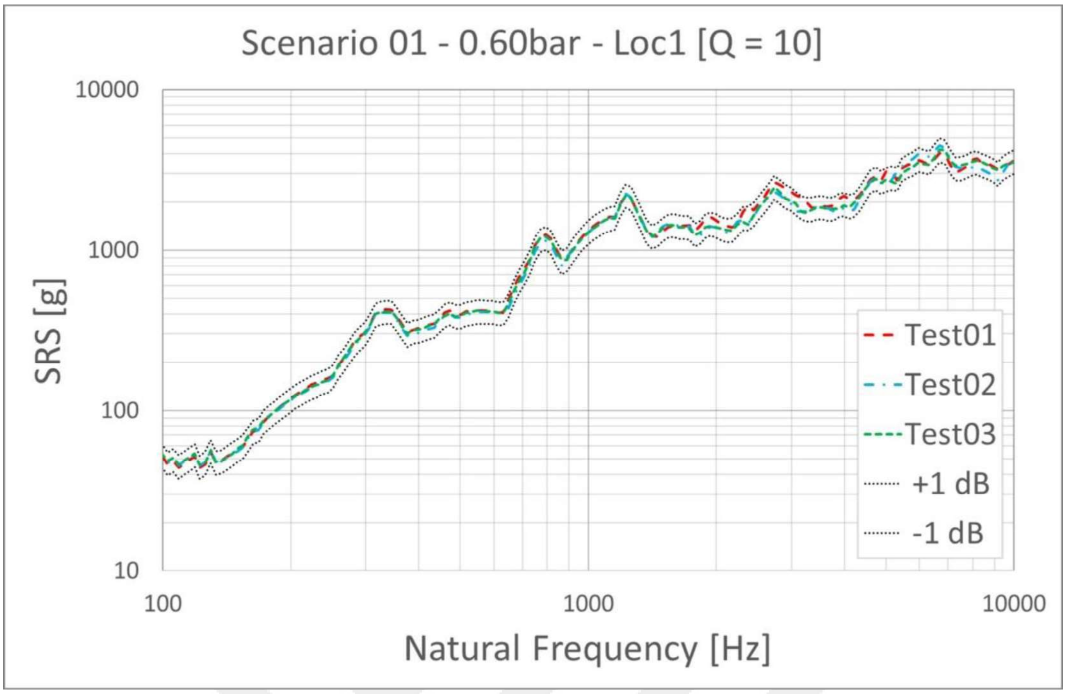
Scenario 01 - 0.60bar - Loc1 [Q = 10]
SRS [g]
Natural Frequency [Hz]
10000
1000
100
10
100
1000
10000
Test01
Test02
Test03
+1 dB
-1 dB

(a)

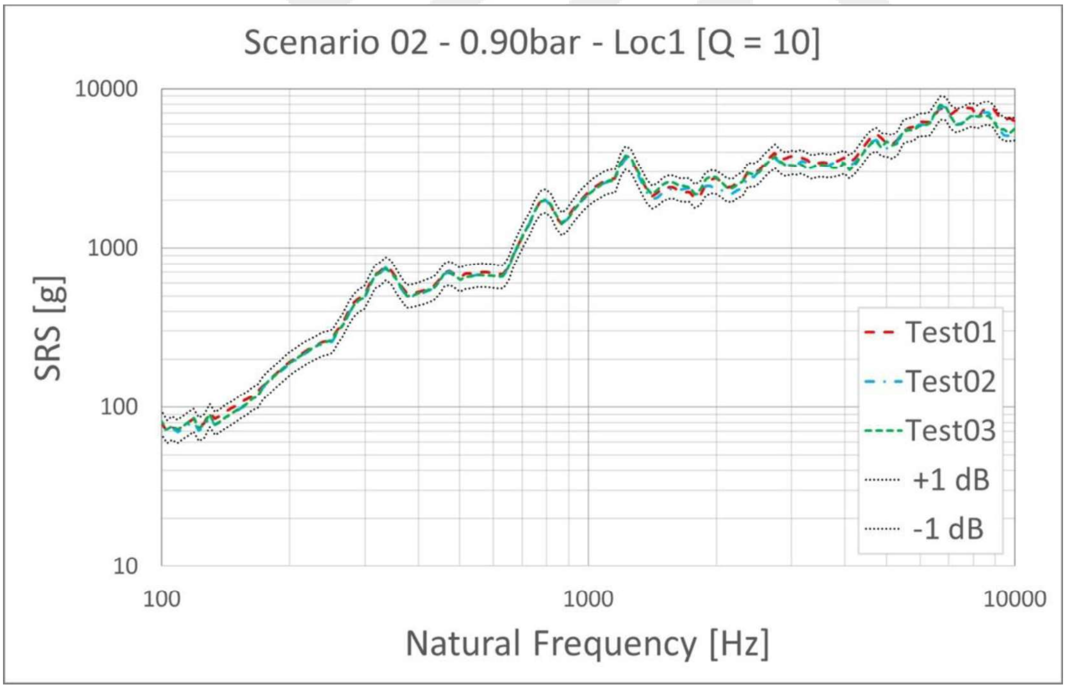
Scenario 02 - 0.90bar - Loc1 [Q = 10]
SRS [g]
Natural Frequency [Hz]
10000
1000
100
10
100
1000
10000
Test01
Test02
Test03
+1 dB
-1 dB

(b)

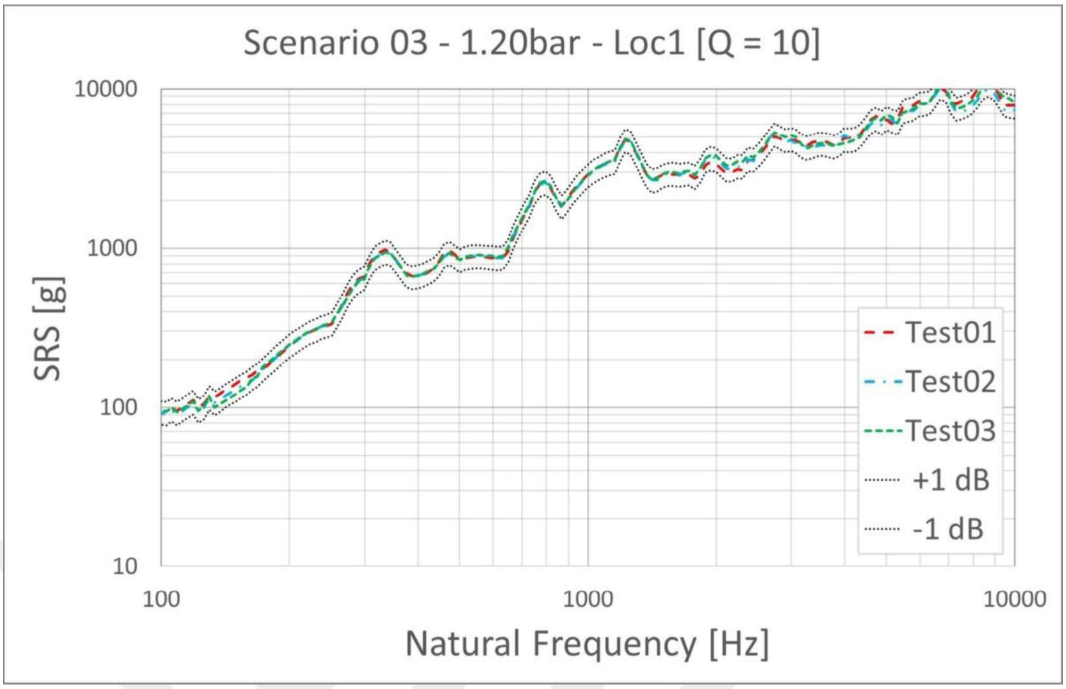
Scenario 03 - 1.20bar - Loc1 [Q = 10]
10000
1000
100
10
SRS [g]
100
1000
10000
Natural Frequency [Hz]
Test01
Test02
Test03
+1 dB
-1 dB

(c)

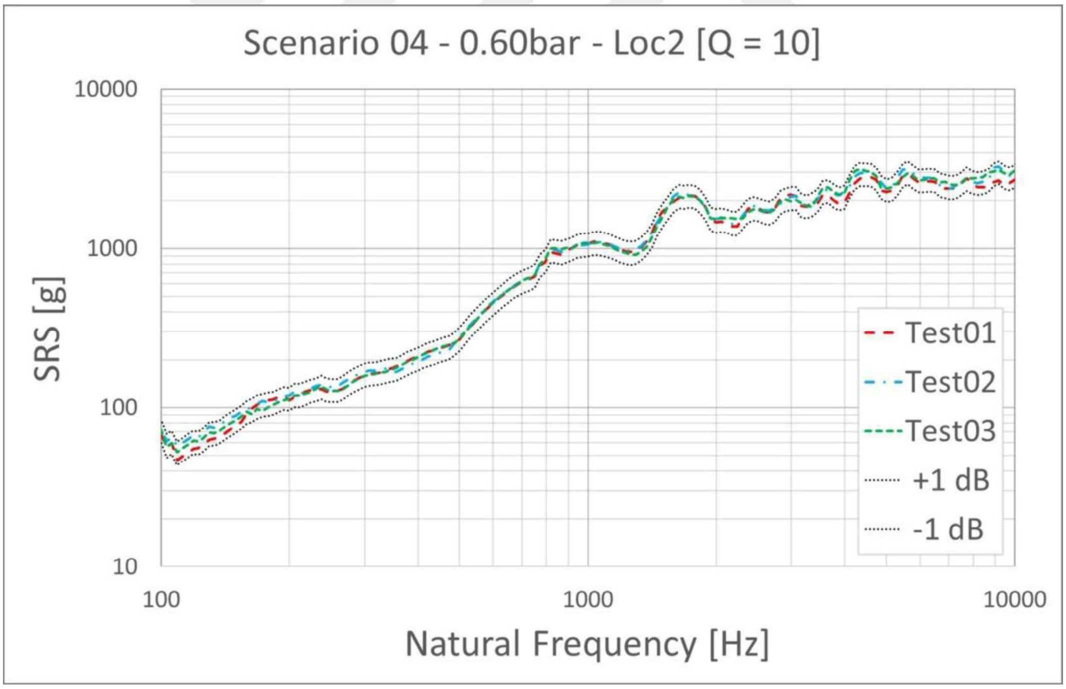
Scenario 04 - 0.60bar - Loc2 [Q = 10]
10000
1000
100
10
SRS [g]
100
1000
10000
Natural Frequency [Hz]
Test01
Test02
Test03
+1 dB
-1 dB

(d)

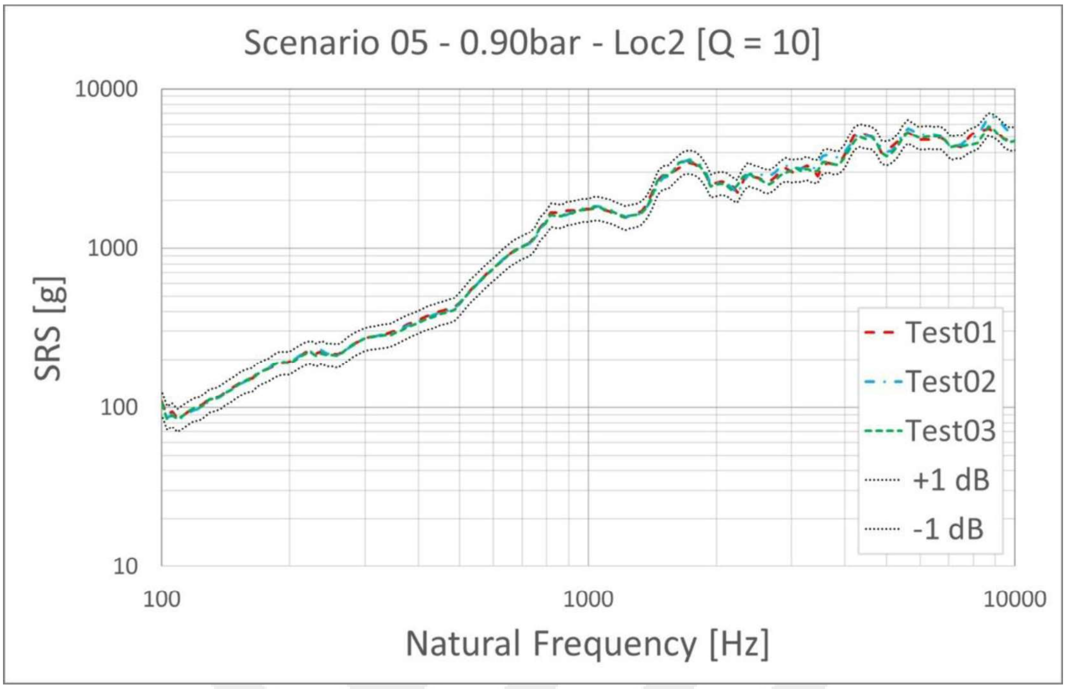

(e)

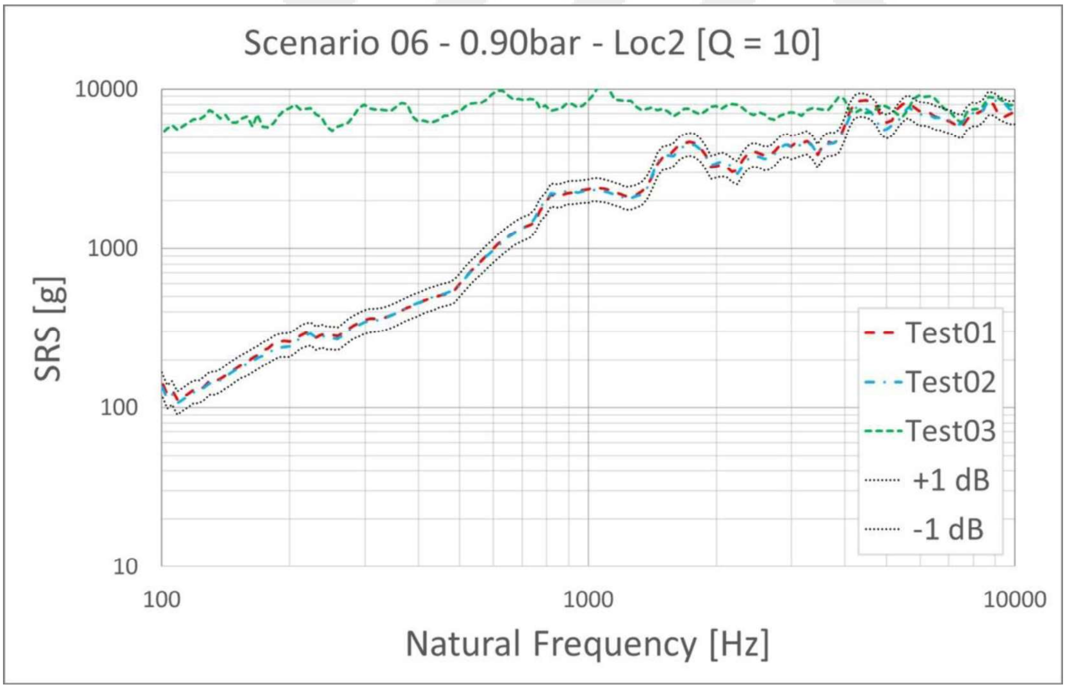

(f)

Figure 3-4. Experimental SRS results obtained from the tests. (a) Scenario 01 (b) Scenario 02 (c) Scenario 03 (d) Scenario 04 (e) Scenario 05 (f) Scenario 06

3.2 Numerical Simulation and Correlation with Experimental Data

As a numerical analysis tool, an explicit finite element solver, LSTC LS-DYNA is preferred in this work. Explicit solvers are superior to implicit ones if highly non-linear loadings and complex nonlinear contacts are present in the model as in the case of the pyroshock test system (see e.g. [47]). However, the results of the explicit finite element analyses should be evaluated carefully since they are conditionally stable and converges if the CFL condition is satisfied. CFL or Courant–Friedrichs–Lewy condition is the necessary condition for convergence while solving certain partial differential equations (usually hyperbolic PDEs) numerically with explicit time integration schemes. Moreover, they present a result whether it is reasonable or not, contrary to implicit non-linear solutions. Therefore, the results should be correlated with the experiments before they are taken into consideration, as done in the current work.

The FE model of the experimental system includes the resonant plate, the projectile, and the measurement adaptor plate used to place the accelerometer, as shown in Figure 3-5. The model mainly consists of reduced integration 2D shell and 3D brick elements. M8 bolts that connect the measurement plate to the resonant plate are modeled with CNRB (Rigid Connection) – Beam Element – CNRB technique. The pneumatic gun and other system elements are not modeled at all for the sake of simplicity. Thus, the projectile is modeled at the very moment of collision. An initial velocity is imposed to the projectile with **INITIAL VELOCITY GENERATION* card of LS-DYNA according to the values measured from the first set of experiments.

Corner springs that support the resonant plate are not included in the FE model and no constraint is imposed to the connection points since in the real system the resonant plate is loosely connected to the supporting bolt-spring system for in-plane directions. It is supported by the springs in the vertical direction but that effect is not modeled as well since it is concluded that they are not effective for acceleration results of the interested points.

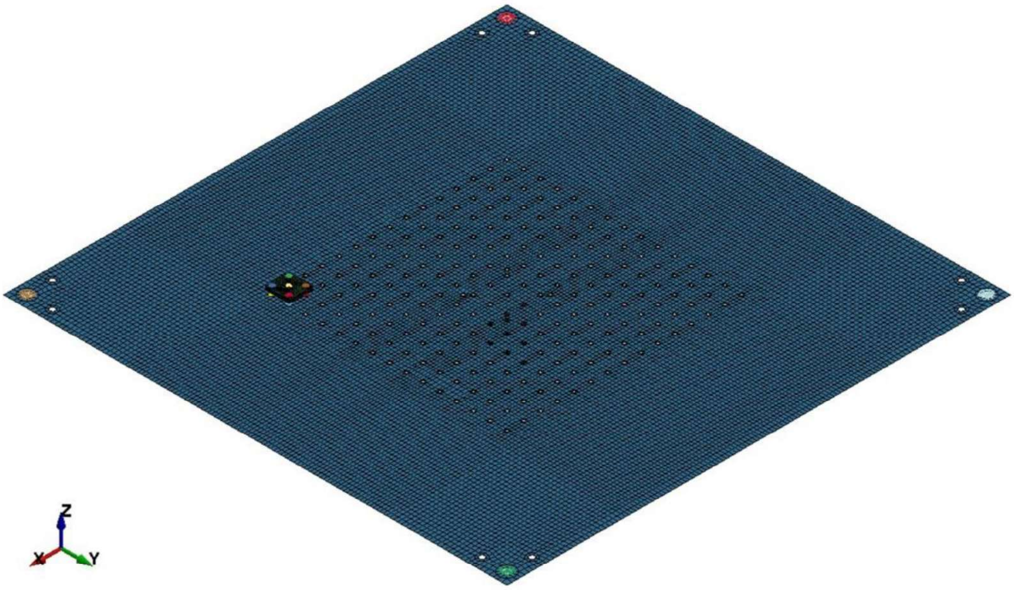

(a)

(b)

Figure 3-5. Finite element model of the experimental setup

The mass of the accelerometer and its stiffness contribution to the system are negligible compared to the other elements, thereby it is not modeled physically. However, a rigid element is added to the hole which is screwed in the experiments and the acceleration data is extracted from the midpoint of this rigid connection element. In this way, it is aimed to average the acceleration of several nodes on the hole surface and to prevent a local unphysical acceleration peak that might arise due to the consideration of just a single node.

Element size differs throughout the model, from 15mm for the projectile to 10 mm for the resonant plate and 5mm for the measurement plate. For the parts where the wave propagation is critical, namely the resonant plate and the measurement plate, the mesh is fine enough to have at least 10 elements per wavelength for the maximum frequency in consideration as recommended in the literature (see e.g. [3]). All materials are modeled as linear elastic since no plastic deformation is expected to occur in the simulations presented in the paper which is valid for the performed experiments as well.

3.2.1 Mesh Convergence Study

An additional mesh convergence study is performed to check the mesh sensitivity of the model although recommended element sizes are preferred in the simulation as mentioned in previous section. Mesh convergence study is considered for the resonant plate, the most critical part of the experimental setup in terms of transmitting the shock wave to the DUT.

Element sizes of 20mm, 10mm and 5mm are considered within the scope of mesh convergence study. Regarding meshes are presented in Figure 3-6, Figure 3-7 and Figure 3-8. As convergence assessment, acceleration – time output of the node representing the sensor is extracted and converted to SRS graph for all cases. Results are evaluated considering ±1dB tolerance band as the test results.

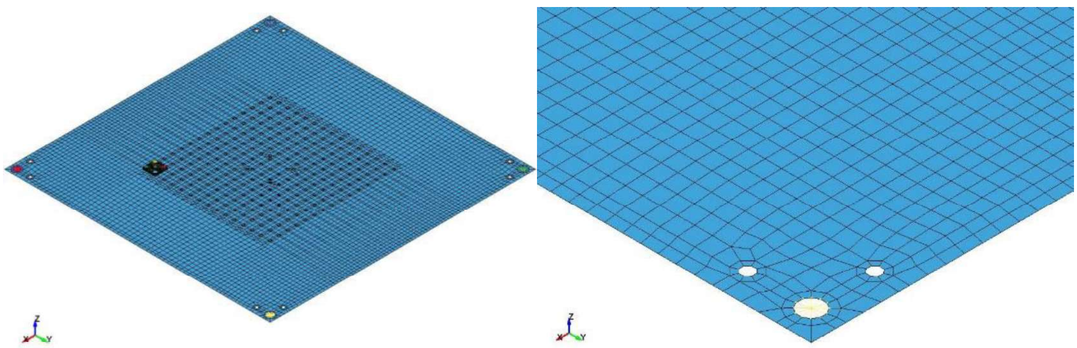

Figure 3-6. 20 mm mesh of the resonant plate

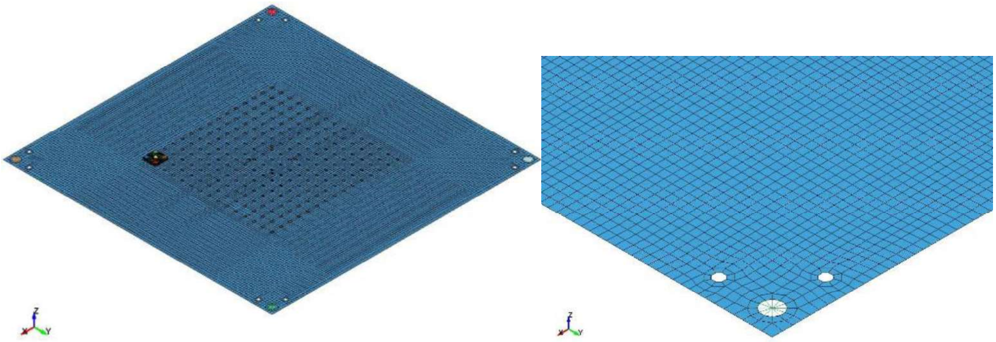

Figure 3-7. 10 mm mesh of the resonant plate

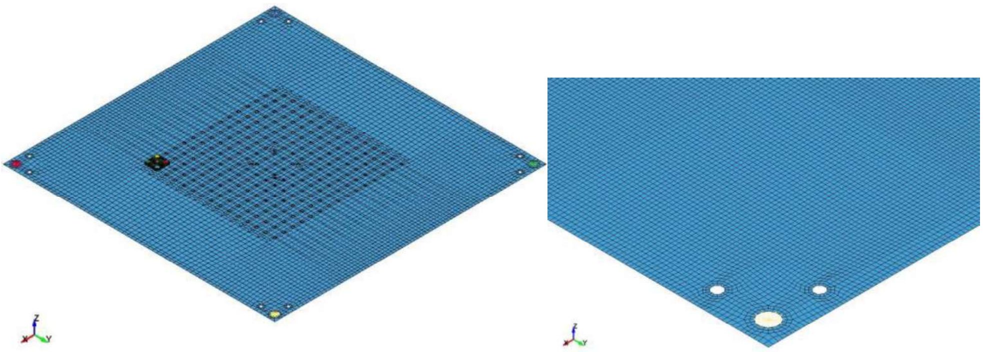

Figure 3-8. 5 mm mesh of the resonant plate

SRS results of the mesh convergence study presented in Figure 3-9. It could be stated that the response of the system is almost same up to 3 kHz frequency level. Between 3-10 kHz, SRS curves are not same though they are in ±1dB tolerance band. Change with different element sizes are random and no valuable relation could be extracted with decreasing element size. In the sense that staying in ±1dB tolerance band as in the physical experiments, it could be concluded that all 3 element sizes, 20, 10 or 5 mm, are suitable for such a simulation. However, in order to have at least 10 elements per wavelength for the maximum frequency in consideration as recommended in the literature, 10 mm element size is preferred.

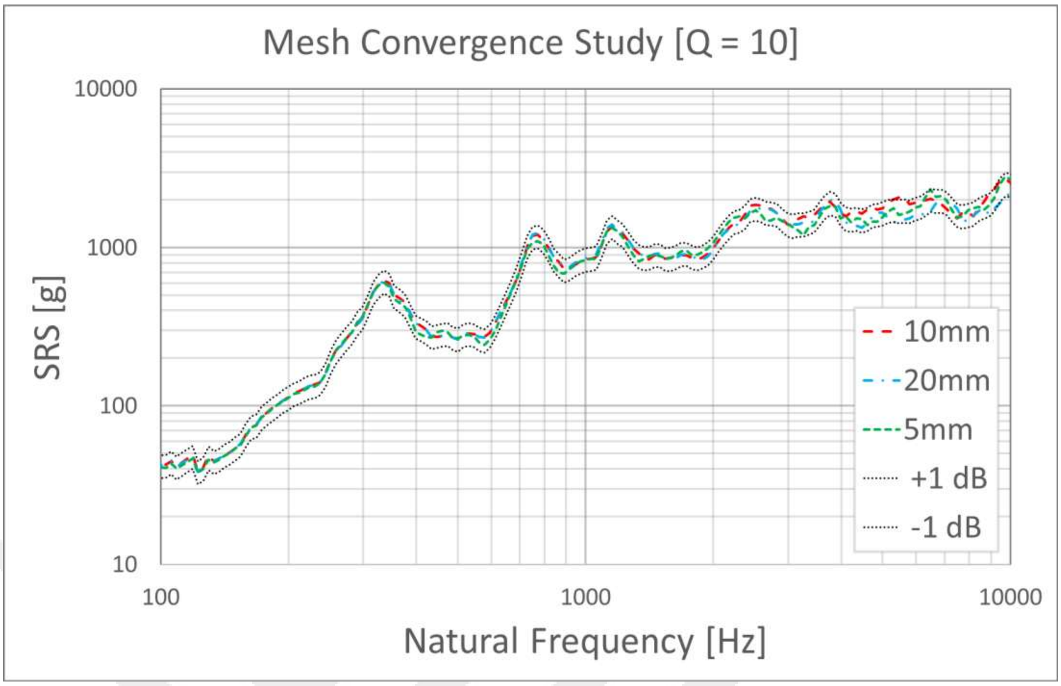

Figure 3-9. SRS outputs of different mesh sizes

3.2.2 Parameter Sensitivity Simulations

The ringing plate type pyroshock test systems are well studied in the literature both experimentally and numerically thus the effects of the test system performance parameters such as projectile weight, resonant plate size and thickness, impact velocity, etc. are well-known and studied in Chapter 2 as well. However, the specifications which have importance for a successful explicit simulation, such as contact and damping parameters are not well-studied and their practical effects in a pyroshock FE simulation – experiment correlation process is not clearly known. Therefore, it is necessary to conduct sensitivity simulations and evaluate the influence of those parameters on SRS curves before the correlation process.

Firstly, the damping parameters are studied thoroughly since they seem to be critical not to overestimate the amplitudes in an SRS curve. Though there are different damping alternatives users can activate, originally LS-DYNA solves an undamped dynamic transient system. One of those options is the classical Rayleigh Damping which is based on the stiffness and the mass matrices of the system. It uses a system damping matrix C defined as:

$C = \mu M + \lambda K$

Where;

μ is the mass proportional Rayleigh damping coefficient,

M is the system structural mass matrix,

λ is the stiffness proportional Rayleigh damping coefficient,

K is the system structural stiffness matrix.

Rayleigh damping is utilized with *DAMPING STIFFNESS and *DAMPING GLOBAL card sets in LS-DYNA. Two sets of analyses are performed with different mass and stiffness matrix ratios by keeping all other parameters constant in order to isolate the effect of the specific damping parameters. The results are evaluated and compared in form of SRS curves extracted from location 1.

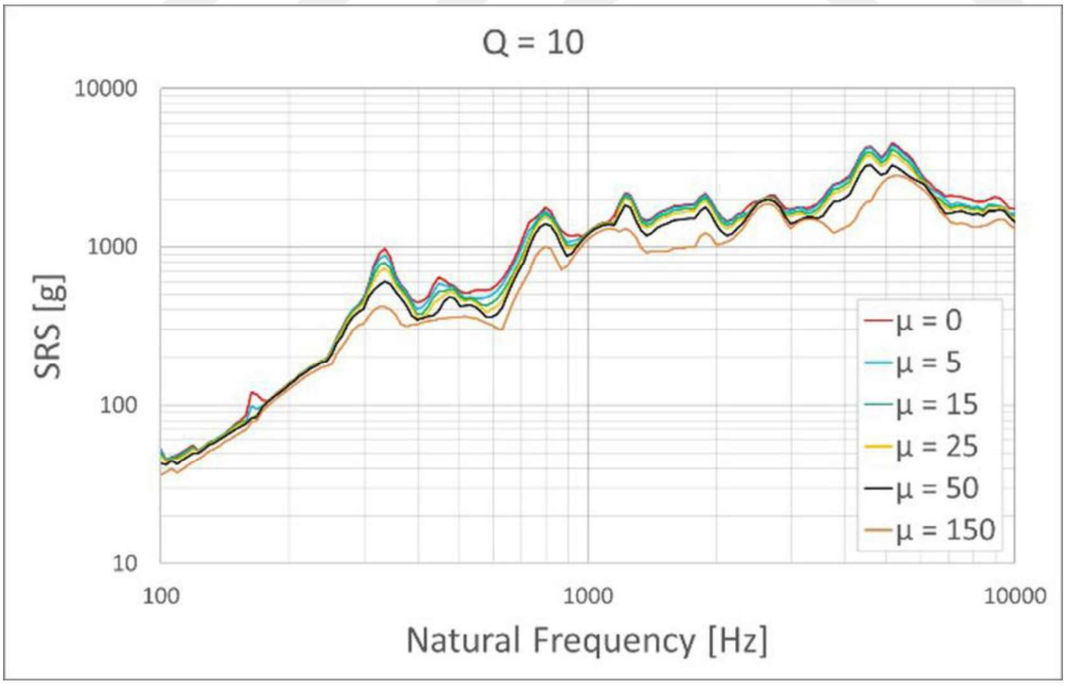

Figure 3-10. Effect of mass proportional damping on the SRS curves

Different values of mass proportional damping are simulated and compared in Figure 3-10 while the stiffness proportional damping parameter λ equals to 0. It is obvious that mass damping decreases the acceleration levels throughout the whole frequency region and it softens the peaks on the SRS curve caused by the natural frequencies of the system. It also causes a shift in the frequency of several peak accelerations but this effect is significant only for high damping levels, as only seen in the μ= 150 damping level.

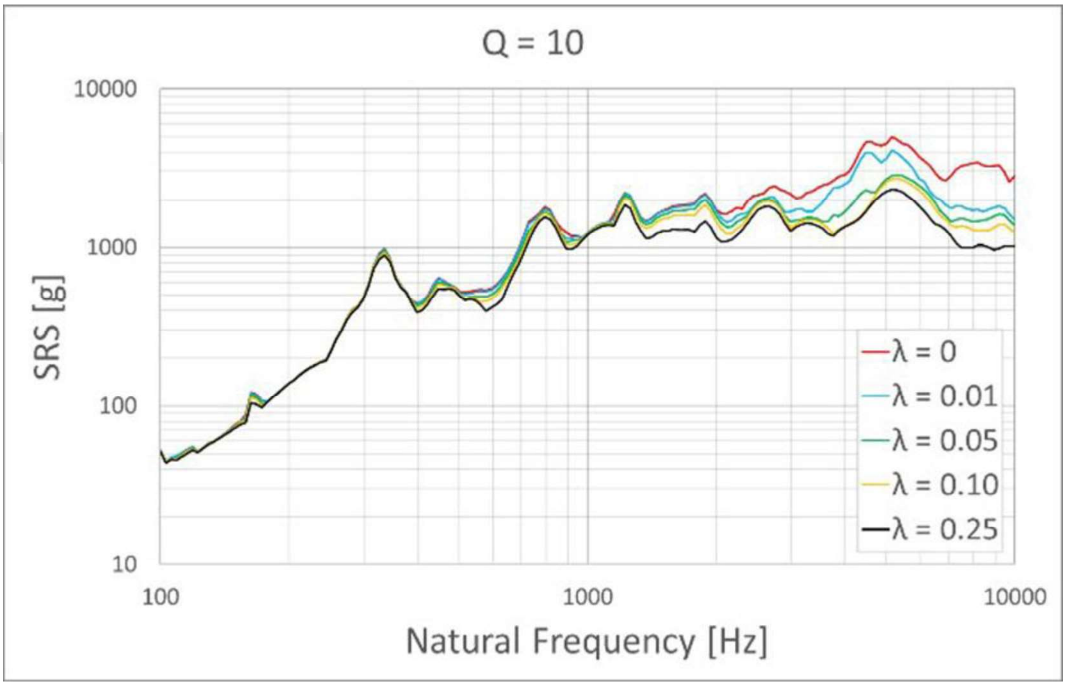

Figure 3-11. Effect of stiffness proportional damping on SRS curves

Various values of stiffness proportional damping are utilized within another simulation set. Contrary to mass proportional damping, the effect of stiffness damping depends on the frequency level and it mostly affects the relatively higher frequency domains as shown in Figure 3-11. The mass proportional damping parameter μ equals to 0 in these simulations. Up to the knee frequency, which is roughly 1 kHz for this test setup, there is minimal influence on the SRS curves. Only the amplitudes on some of the troughs decrease in that frequency range. However, it has a gradual effect after the knee frequency in the form of decreasing the amplitude and smoothing over the peaks. At the high damping levels, it even turns the data to a plateau and all its characteristics are lost from the value of λ=0.25 at frequencies higher than 7.5 kHz.

In the FE computations of pyroshock systems, the load transfer issue requires special attention, i.e. transferring the load between the plates only via fasteners does not reflect the reality. It is vital to have surface-to-surface contact for all touching surfaces. It is observed in the experimental analysis that the different assembly configurations, such as assembling the measurement plate with 3 bolts instead of 4 or assembling by placing additional bushes to prevent the contact between the plates result in different SRS curves. For the simulation model presented in this section, there are 2 interfaces, i.e. the ones between the projectile and the resonant plate and between the resonant plate and the measurement plate. A penalty-based contact algorithm, *CONTACT AUTOMATIC SURFACE TO SURFACE card is utilized for both contact regions. It is based on a logic where springs are placed between the penetrating node of touching (slave) part and the penetrated surface of touched (master) part so that the springs create forces that push the nodes out of the penetrated surfaces (see Figure 3-12). It is a double sided contact algorithm which checks the nodes of slave part against the segments of master part and vice versa. Formulas of contact stiffness values of master and slave side, k_m and k_s, are presented below.

$$k_m = \frac{(SFM)KA^2}{V} \ and \ k_s = \frac{(SFS)KA^2}{V}$$

where

SFM is the penalty scale factor of master part

SFS is the penalty scale factor of master part

K is the bulk modulus of material

A is the segment area

V is the element volume

Since the stiffness of the spring directly affects the amplitude and the frequency content of the transmitted force from one surface to the other, it is critical to have the correct stiffness values for them. Different contact stiffness values are studied through SFS and SFM parameters which directly scale the default contact stiffness calculated by LS-DYNA.

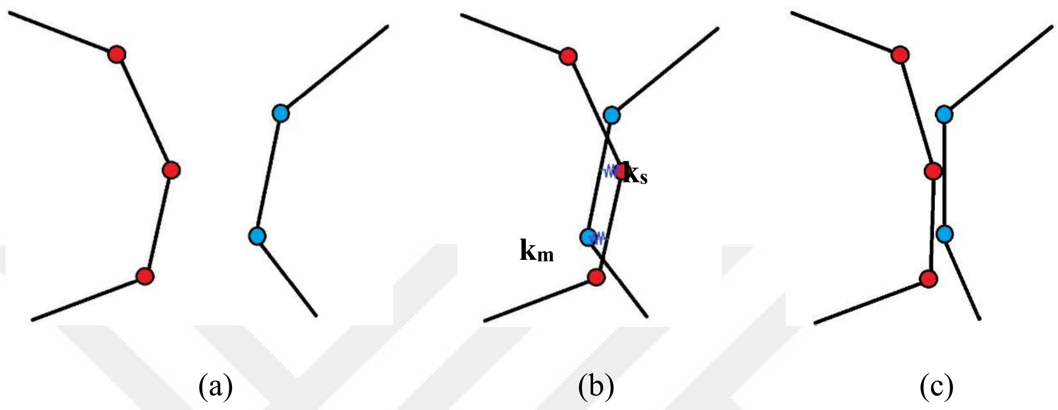

Figure 3-12. Node-to-surface contact algorithm (a) No contact (b) Penetration and imaginary springs. (c) Corrected penetration with spring force.

Simulations for the contact stiffness scale factor of 5, 50, 0.2, and 0.02 are performed and compared with the default value which is the no scaling case in Figure 3-13. The parameters are changed for both contact interfaces equally.

The contact stiffness changes the resulting SRS curve dramatically as presented in Figure 3-13. At the low-frequency range, between 100Hz – 250Hz, the change has a negligible effect, while for the higher values the overall amplitude increases with the increasing contact stiffness. The effect is more dramatic for the high-frequency region. However, the contact stiffness and the amplitude are not directly proportional and the dependence is quite complicated. It is different for every frequency band and every scaling level. For instance, multiplying with 0.20 still keeps the general trend of default stiffness with lower amplitude but multiplying with 0.02 creates an increasing trend between 7 kHz – 10 kHz even though overall amplitudes are much lower than the rest. The outcome of the sensitivity simulations and the values of the discussed numerical parameters and their effects are taken into consideration for the explicit FE simulations of the pyroshock experiments which are presented in the next section.

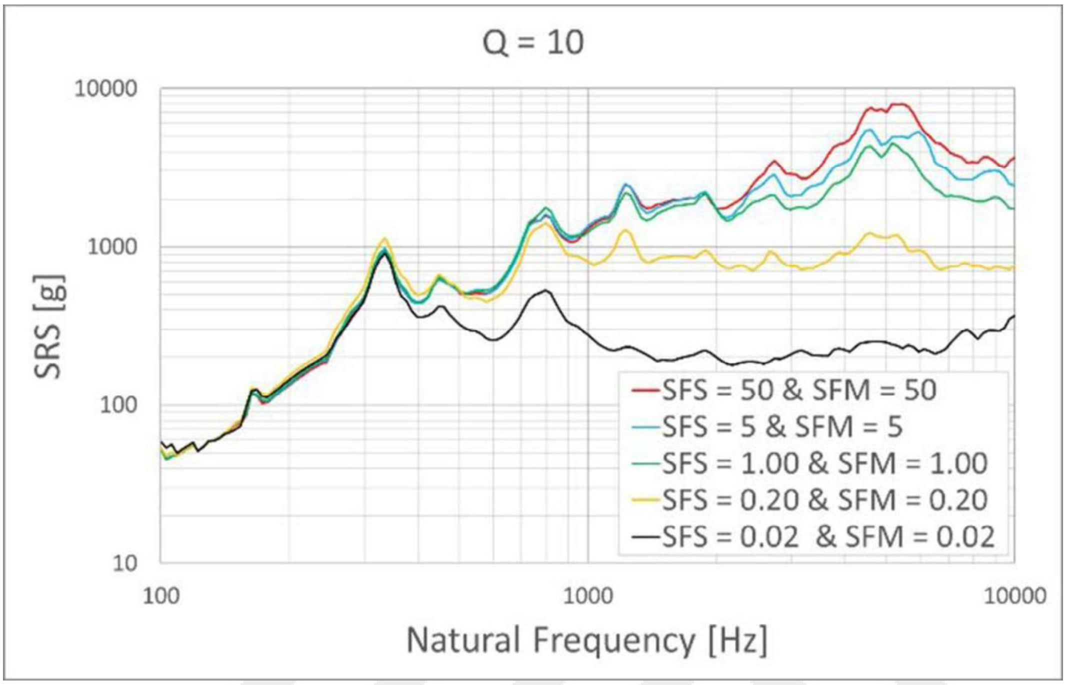

Figure 3-13. Effect of contact stiffness on the SRS response

3.2.3 FE Model Calibration Simulations

Several explicit FE simulations are performed for each test scenario presented previously to obtain a numerical framework representing the real test case with acceptable errors. As a starting point, the simulations for all six scenarios are performed with Parameter Set 01, which is the default contact parameters and no damping at all. Those simulations are labeled as PS01 and the results are presented in Figure 3-14 for different scenarios. A short evaluation reveals that the results show a fair similarity with the experiments. However, for the lower frequency, even though the peaks coming from natural frequencies of the resonant and the measurement plate seem to be captured, the amplitudes at those points are slightly different due to the damping existing in the real test system. For the high-frequency regime, the amplitudes are different not only at the peak points but also in the overall amplitude of the SRS curve. Moreover, while the trend of the SRS curves in the simulations are decreasing the ones in the experiments are not. Considering the fact that there is no damping exists in the FE models with PS01, it is concluded that the two contact interfaces numerically damp the high-frequency content of the transmitted force. As mentioned before, a penalty base contact algorithm has no physical background for the force transmission, it creates fictional springs to represent the applied force of the touching surface.

Since one of the main purposes of this study is to show and to evaluate the modeling potential of explicit FE simulations for a ringing plate pyroshock test system, the optimal parameter sets for damping and contact algorithm are obtained through a manual try-and-check parameter identification and the related results are labeled as PS02 and presented in Table 3.3. The simulations for all six scenarios are performed again and the comparison is presented in Figure 3-14 as well.

Table 3.3 Simulation parameter sets

Parameter Set	Mass Proportion Damping Coefficient (μ)	Stiffness Proportion Damping Coefficient (λ)	Contact Stiffness (SFS)	Contact Stiffness (SFM)
PS01 (Default)	0	0	1	1
PS02	25	0.005	25	25

The simulations with the PS02 parameter set shows significant differences from the ones performed with default parameters. First of all, the peaks which indicate the natural frequencies of the system up to 900Hz decrease and get closer or even identical with the experimental results. For location 1 (Scenario 01-02-03), there are two significant peaks which are around 330 Hz and 650 Hz. The new set of simulations catch the peak values exactly for the latter and although there still is a gap between the simulation and the experiment, it reveals a closer value for the former. As an unexpected outcome, it decreases the amplitude of the SRS curve between 300 Hz – 500 Hz and it is debatable that the new damping parameters shift the modal density in that range. For location 2 (Scenario 03-04-05), both peaks which are around 180Hz and 800 Hz are eliminated and the results overlap almost perfectly. There is no unexpected decrease for that location. After the knee frequency, there is a remarkable difference between 5 kHz – 10 kHz for all scenarios between PS01 and experimental results. Apart from that, there are some small discrepancies throughout 900 Hz to 5 kHz, which are more apparent for 0.60 bar cases (Scenario 01 and 04). PS02 results show that the simulation – experiment curves match much better for 5 kHz – 10 kHz region with some overshoot for 0.90 bar and 1.20 bar cases (Scenario 02-03-05-06). However, for 0.60 bar (Scenario 01 and 04), although the amplitude of the curves increases between 7 kHz – 10 kHz, they are still well under the experimental results.

It is concluded that increasing the contact stiffness enhances the transmission of the high-frequency content of the impact force but this effect diminishes with decreasing impactor velocities. Thus, further increase of the contact stiffness parameters will work better for those cases but it also increases the level of accelerations for 0.90 bar and 1.20 bar simulations which would lead to a mismatch with the experimental results. Even though it is not considered here a variable contact stiffness parameter with respect to impact velocity could lead to better results.

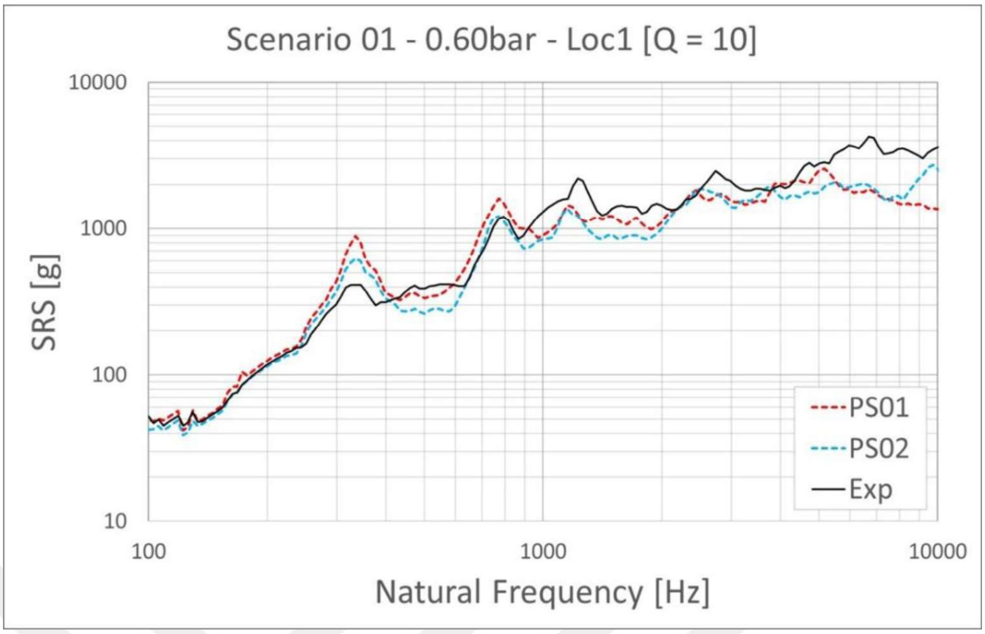
Scenario 01 - 0.60bar - Loc1 [Q = 10]
SRS [g]
Natural Frequency [Hz]
10000
1000
100
10
100
1000
10000
PS01
PS02
Exp

(a)

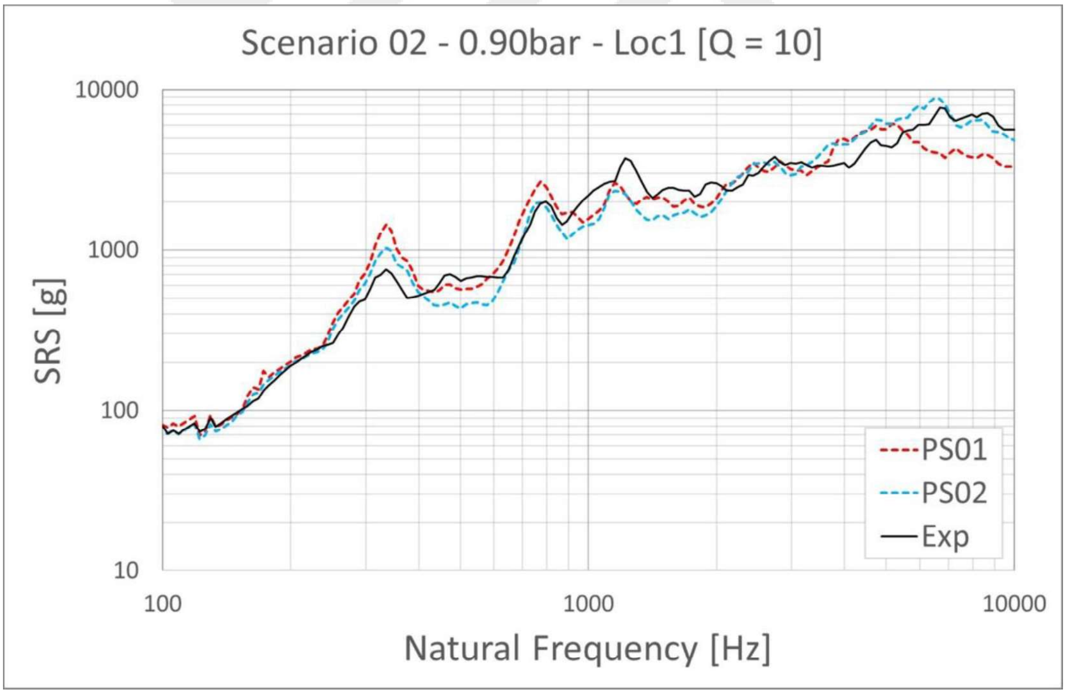
Scenario 02 - 0.90bar - Loc1 [Q = 10]
SRS [g]
Natural Frequency [Hz]
10000
1000
100
10
100
1000
10000
PS01
PS02
Exp

(b)

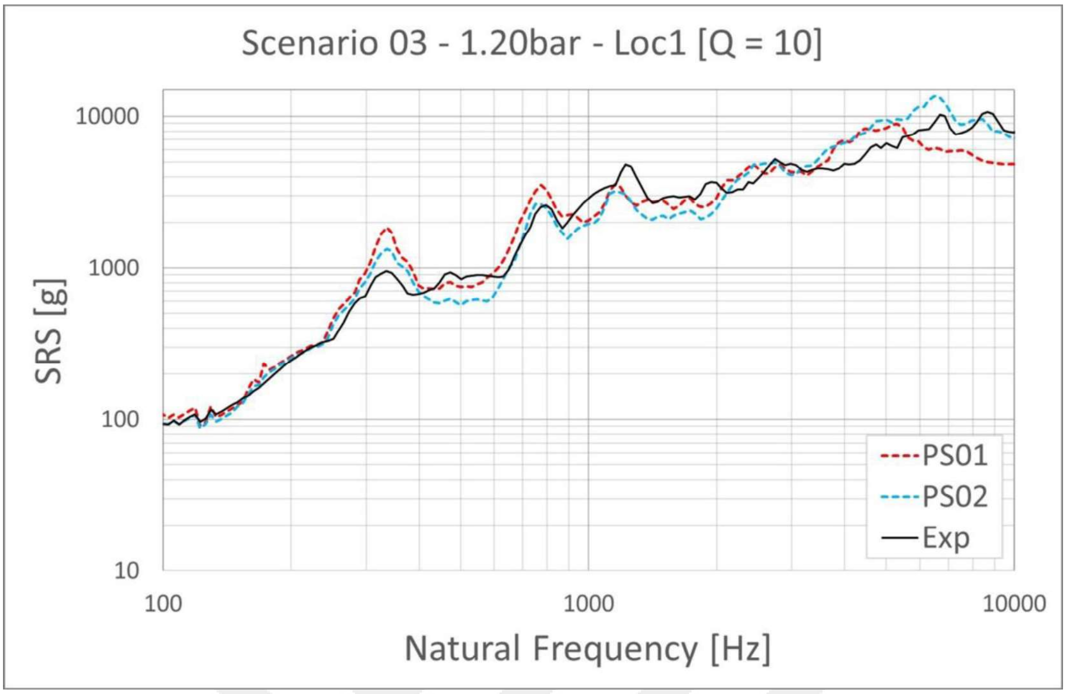
Scenario 03 - 1.20bar - Loc1 [Q = 10]
10000
1000
100
10
SRS [g]
100
1000
10000
Natural Frequency [Hz]
PS01
PS02
Exp

(c)

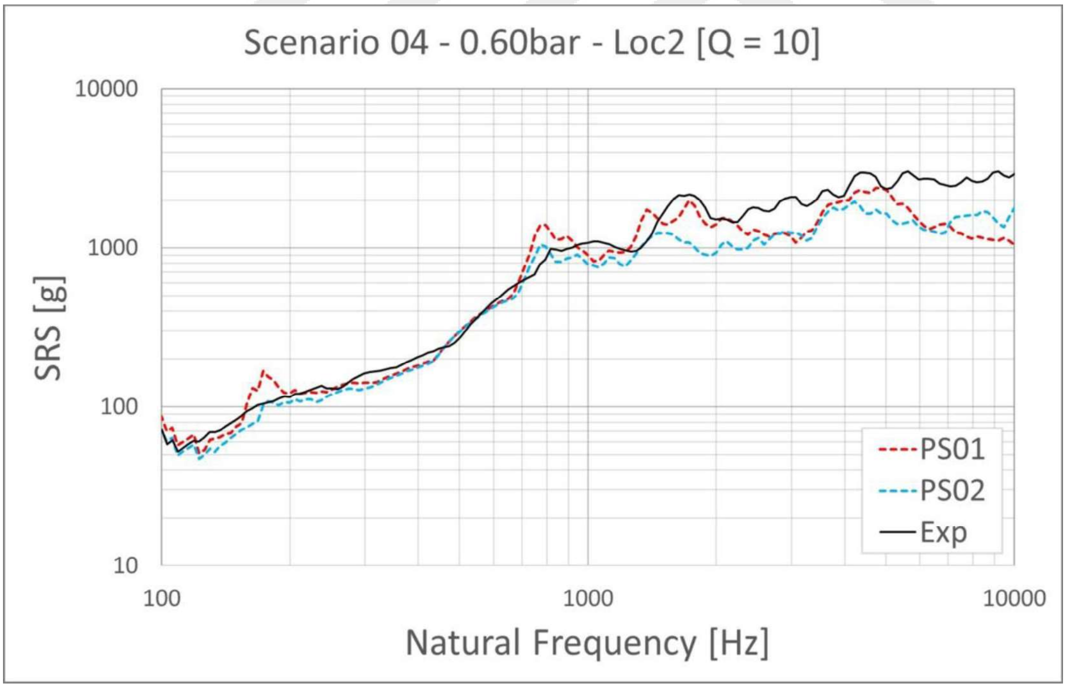
Scenario 04 - 0.60bar - Loc2 [Q = 10]
10000
1000
100
10
SRS [g]
100
1000
10000
Natural Frequency [Hz]
PS01
PS02
Exp

(d)

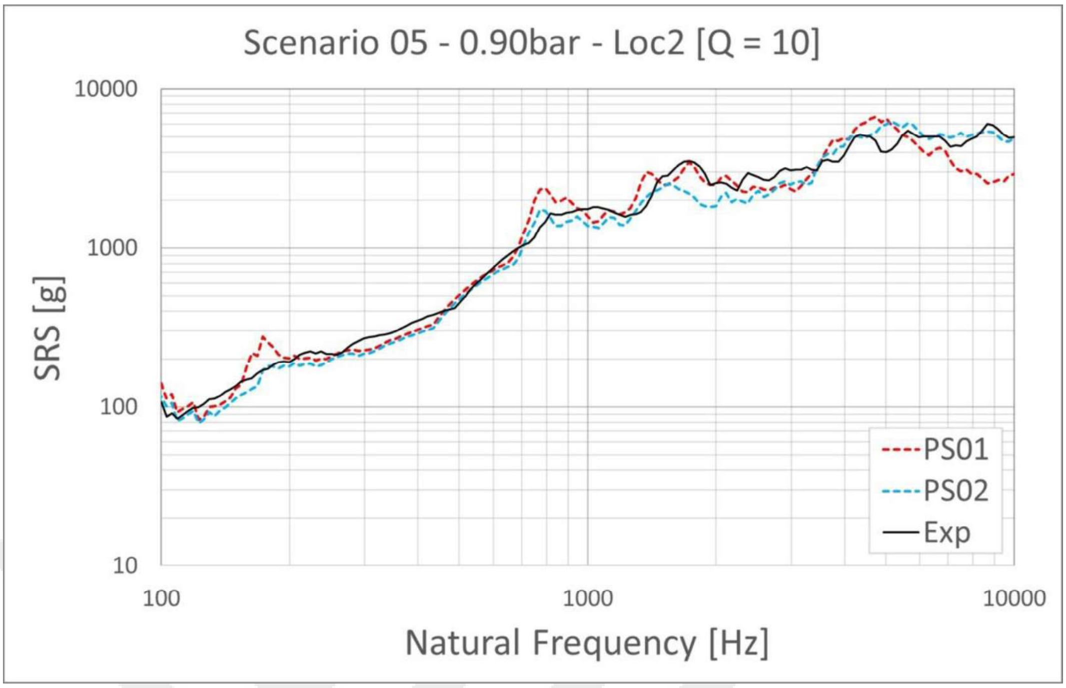

(e)

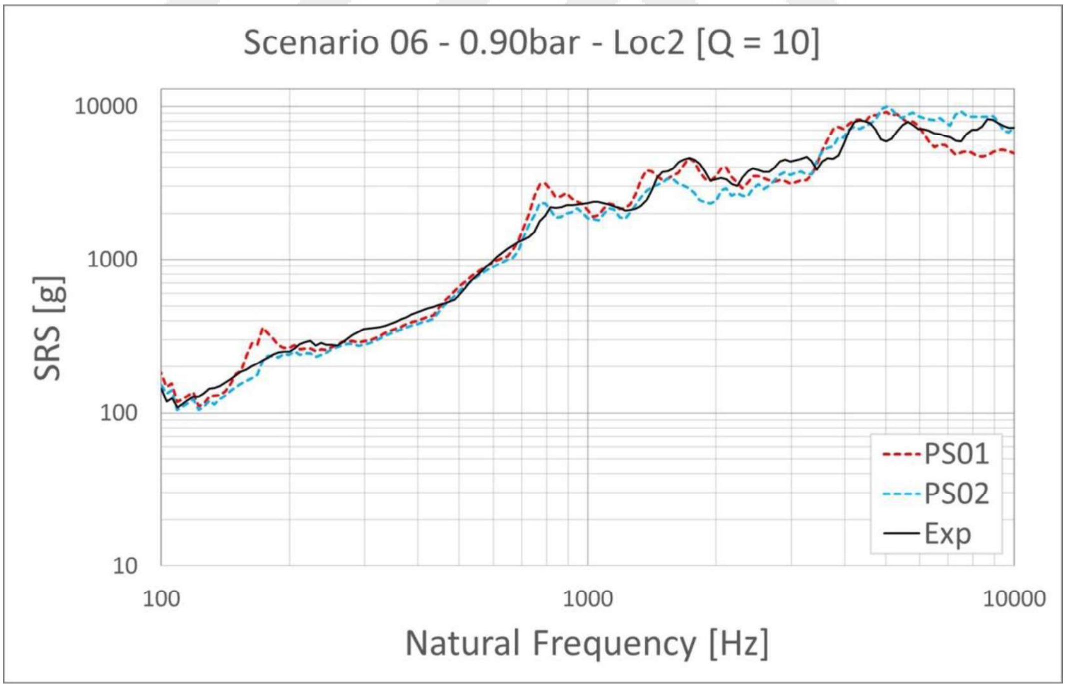

(f)

Figure 3-14. Comparison of experimental and numerical SRS results

CHAPTER 4

NUMERICAL SIMULATIONS FOR TESTING PARAMETER CALIBRATION PROCESS

4.1 Methodology and Aim

The experimental and the numerical studies are presented with a focus on FE computations – experiment correlation of the ringing plate test system throughout Chapter 3. For the sake of simplicity and illustration of the effect of different parameters, the study has been conducted without any DUT mounted on the test bench. The performance of the explicit FE computations and possible improvements on the default parameters are evaluated. In this Chapter, the outcomes from previous sections are applied at a real qualification pyroshock test case which includes a dummy instrument mounted on the test bench. The primary aim of the test is to create the pyroshock environment that the device will undergo in its service life and qualify the instrument that it will withstand the pyroshock loads.

It is critical to evaluate the performance of explicit FE simulations for a test case with an instrument mounted in order to check the potential of explicit FE simulation to speed up the trial-and-error phase of the ringing plate test system.

4.2 Case Study for a Dummy Equipment

Metal-to-metal impact type pyroshock test setups are able to mimic a real pyroshock loading to an instrument but they require special attention (see e.g. [8]) since the test systems are quite sensitive to all kind of inputs including not only pneumatic gun pressure, mass and geometrical properties of resonant plate and impactor but also assembly type of the instrument, torque levels applied to the fasteners or the error in the flatness of the adaptor plate. Thus metal-to-metal impact type test setups require considerable trial-and-error effort using a dummy DUT to achieve the specified qualification level SRS for the excitation into the instrument mounted [38, 42]. In order to prevent the over-testing of the real instruments through the error-and-trial process, the pyroshock test is therefore performed initially with such representative dummy instruments, which is a common application to ensure that the real instrument is exposed just the necessary shock levels. The Dummy instrument should have the same interface to the resonant plate, the same center of gravity, and a similar moment of inertia as well as a similar structure with the real instrument. In this study, it is a rectangular-shaped instrument and connected to the resonant plate via a thick adaptor plate with the help of M6 bolts. An overview 3D representation of the dummy instrument is presented in Figure 4-1.

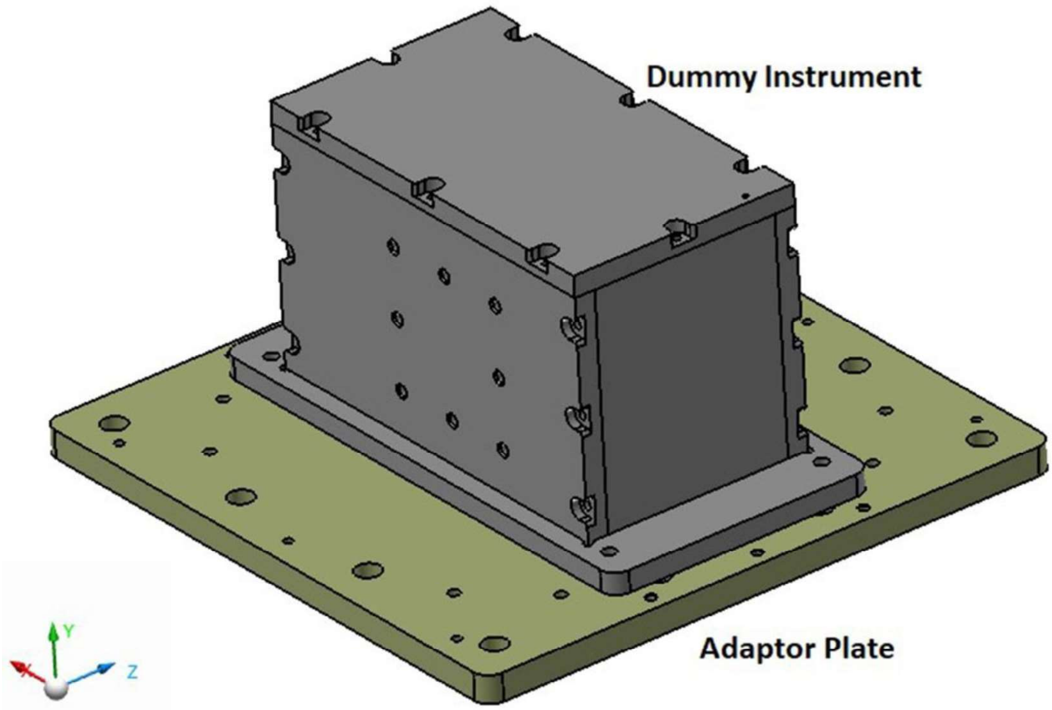

Figure 4-1. CAD representation of dummy ınstrument

4.2.1 Numerical Simulations

The finite element model is developed like in the previous case without a dummy instrument, where the 2D shell and 3D brick reduced integration elements with linear elastic material definitions are used and illustrated in Figure 4-2. All fastener connections except the ones within the dummy instrument are modeled with CNRB (Rigid Connection) – Beam Element – CNRB technique. The mesh size for the dummy instrument and the adaptor plate is 5 mm. In FE simulation, the improved parameter set, PS02, is utilized for damping and contact parameters. The results of the simulation are presented in Figure 4-4 in comparison to experimental data.

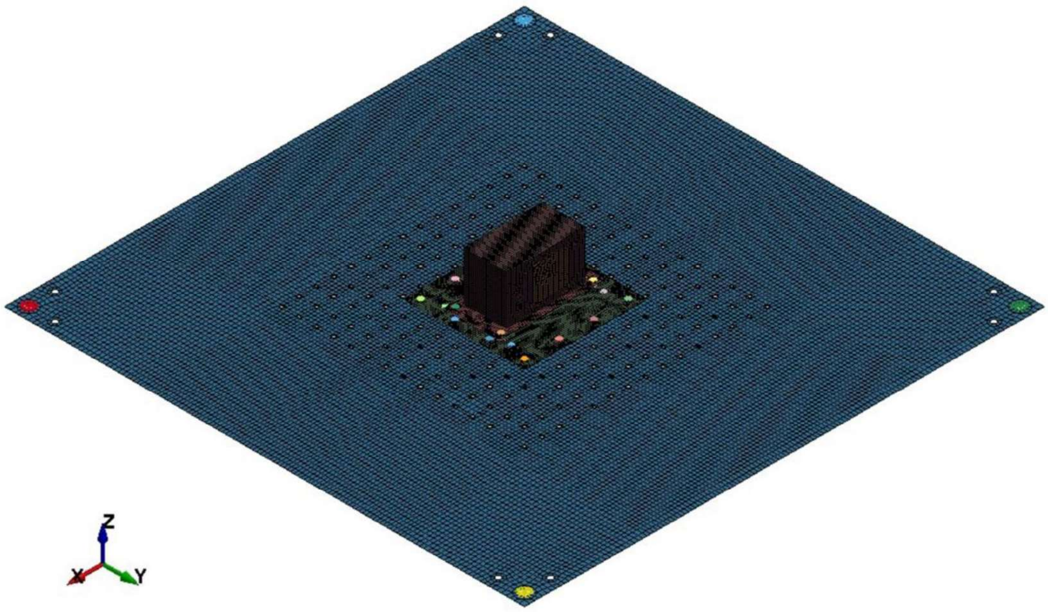

Figure 4-2. Finite element model with the dummy instrument

4.2.2 Experimental Simulations

The Pyroshock test presented in this section is one of the trial-and-error tests with the dummy DUT. It is performed to check whether the qualification level pyroshock loading can be simulated. Qualification level test is defined as the test which is performed on a hardware item that will not be flown but manufactured using the same drawing, materials, tooling, processes, inspection methods, and personnel competency as used for the flight hardware. The purpose of a qualification test is to verify the design integrity of the flight hardware with a specific margin [6] and it is well known that the design of the equipment of the spacecraft must retain a qualification load scenario that is higher than the operative one [25]. The test is performed with a 15 kg impactor at a pressure level of 1.80 bar. Whole dummy instrument – adaptor plate assembly is mounted on nuts via bolt connection points in order to prevent direct contact between the adaptor plate and the resonant plate. With this assembly technique, the modal coupling is prevented to a certain extend and the modal density is decreased mostly for the high-frequency region in order to stay in the band of tolerance levels of the desired pyroshock loading. This is a version of multiple resonant plate application named as bi-plate and exists in literature (see e.g. [37]).

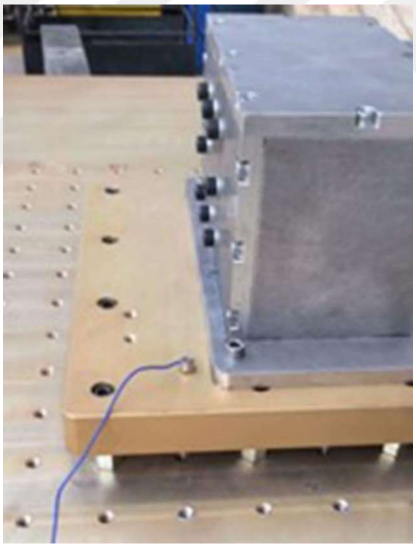

Figure 4-3. Accelerometer and the dummy instrument

Acceleration – time data is measured by a piezo-resistive type single-axis shock accelerometer as in the previous experiments. It is mounted on the adaptor plate at a very near point to one of the four bolt connection of the dummy instrument, as shown in Figure 4-3. Measured data is converted to SRS curve and shown in Figure 4-4 together with the qualification shock level. A tolerance limit of +6 dB / -6 dB is established for the desired shock level [42]. The repeatability of the system is checked previously, therefore the analysis is conducted here through a single experiment.

The experimental SRS curve does not exactly match with the described qualification shock level but it is in the tolerance levels.

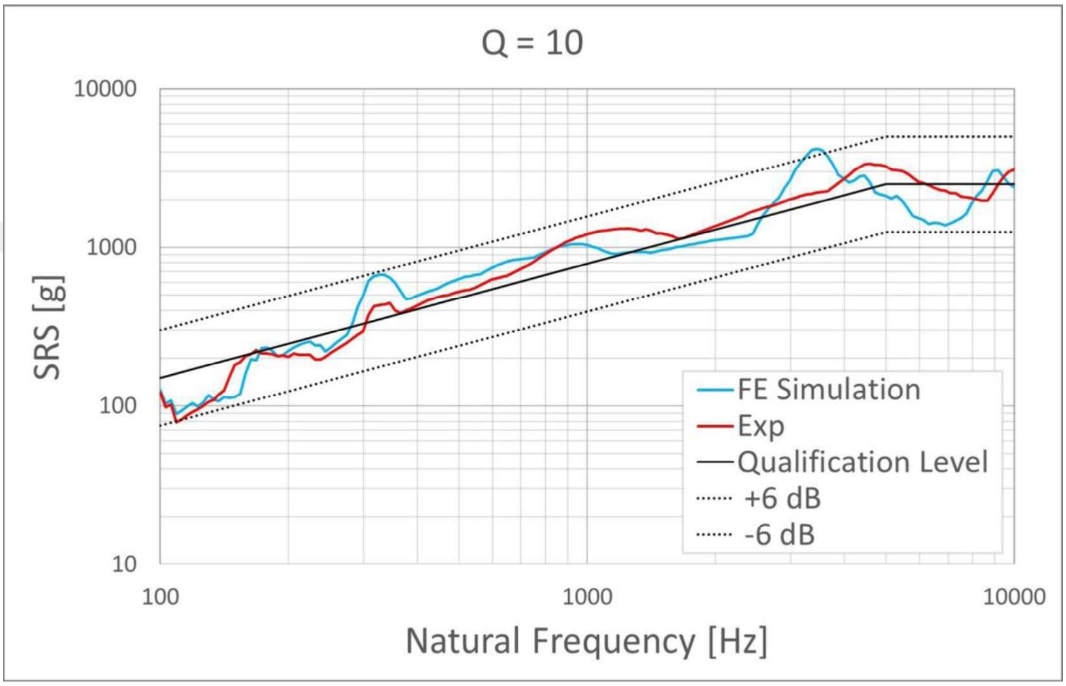

Figure 4-4. Experimental and numerical SRS results of the test with the dummy instrument

As depicted in Figure 4-4, the general trend of the SRS curves of experimental and numerical results agree with each other. With a closer look at the low to mid-frequency region, there are 2 peaks around 180 Hz and 320 Hz within both experimental and numerical results. Numerical results catch the amplitude of the first peak but not at the correct frequency, there is a shift towards lower frequency. For the second one, it is vice versa, the peak is captured at the correct frequency but the amplitude is much higher for the experimental result. In the mid-field frequency region, knee frequency is captured with approximately 10% error. It is at 1 kHz for the experimental result but 900 Hz for the FE result. It could be concluded that FE simulation results agree with the experimental results in general. Except for some frequency shift and amplitude over estimation around 320 Hz, the trend and all peaks and troughs of the experimental SRS curve in low and mid-frequency ranges are captured.

In the high-frequency region, the trends agree with each other but there is a certain frequency shift for the sinusoidal-like behavior of the curve between 4 kHz – 10 kHz as well as the amplitude around the beginning of sinusoidal-like shape is overestimated by numerical results. It shows a lower amplitude between 4 kHz – 8 kHz and catches the amplitude after 8 kHz. Recalling the main purpose of this work, contrary to the differences between numerical and experimental results, SRS curves agree with each other to an extent that gives confidence to users to conduct solely numerical simulations to have an estimate on the behavior without extended experimental studies. Experimental setup and production errors of the dummy instrument might be the cause of the differences as well as the limitation of numerical simulation itself. It is observed that even small variations in the applied torque levels to the M6 fasteners at the interface of the dummy instrument lead to certain differences in the experimental SRS curves.

CHAPTER 5

CONCLUSION

The main objective of this thesis work is to show and evaluate the potential usage of the explicit FE simulations for a metal-to-metal impact pyroshock test bench. FE simulations are proposed to use in two different stages. First, they are used to estimate the effects of different design parameters at the conceptual design phase for a ringing plate test system, as it is done in several studies in the literature. Secondly and more importantly, FE simulations are evaluated for trial-and-error phases of open-loop pyroshock test systems as in the case of the ringing plate test system. Simulations are performed with the default and improved parameter sets and compared to the experimental results. All correlation processes, including parameter sensitivity simulations and simulations of the performed experiments with different parameter sets, are studied without any DUT for simplicity. After the agreements obtained between the numerical and the experimental SRS curves, the explicit FE simulation performance is evaluated for a dummy mounted real trial-and-error test case. The main outputs of this study could be summarized as follows:

- Explicit FE method has a valuable potential to predict shock levels on a ringing plate type pyroshock test bench.
- As Lee et al. mentioned in their review, the implicit FE method, considering accurate and detailed modeling, shock simulation for the simple model showed good SRS predictions compared to the test-measured SRS at low frequencies [10]. Contrary to the implicit FE method, the explicit FE approach is in good agreement with the test results for the frequency range greater than 5 kHz with the help of calibrated damping and contact parameters.
- The explicit FE method could be a powerful tool for the shock level calibration tests with a dummy instrument beforehand, the pyroshock test of

the real instrument. It could lower the necessary test number from hundreds to tens or even less.

The structures and systems need to withstand the qualification level pyroshocks throughout the mission to prevent possible system failures considering the importance of the instrument and the system level pyroshock tests for space programs. The instrument-level ringing plate pyroshock tests could be more effective in terms of time and labor with a powerful tool in hand to predict testing parameters to achieve the desired qualification shock level.

As a further study, the calibrated simulation parameters' performance could be checked with different DUT and different test systems. Instead of a constant parameter set, they could be formulated as functions that depend on impact speed, material type, and test bench type to achieve consistent and high-fidelity results in general.

REFERENCES

[1] Alexander, J. E. (2009). The shock response spectrum - A primer. Conference Proceedings of the Society for Experimental Mechanics Series, 43(6), 6-14.

[2] Department of Defense of United States of America (2019). Environmental Engineering Considerations And Laboratory Tests (MIL-STD-810H).

[3] ECSS. (2015). Space engineering: Mechanical shock design and verification handbook (ECSS-E-HB-32-25A).

[4] Harris, C. M., & Piersol, A. G. (1962). Harris' Shock and Vibration Handbook. New York, NY: R. R. Donnelley & Sons Company.

[5] Kunicka, B. I. (2016). Spacecraft dynamic analysis and correlation with test results. Luleå University of Technology, Noordwijk.

[6] NASA. (2011). Pyroshock Test Criteria (NASA-STD-7003A).

[7] Lake, E. R., Thompson, S. J., & Drexelius, V. W. (1973). A study of the role of pyrotechnic systems on the space shuttle program (CR-2292). Washington D.C.: Mcdonnel Douglas Corporation.

[8] Bement, L. J., & Schimmel, M. L. (1995). A manual for pyrotechnic design, development and qualification (110172). Virginia: NASA.

[9] C.J. Moening. (1985). Pyrotechnic shock flight failures. Proceedings of Institute of environmental sciences pyrotechnic shock tutorial program, in: 31st Annual Technical Meeting of the Institute of Environmental Sciences (IES).

[10] Lee, J. R., Chia, C. C., & Kong, C. W. (2012). Review of pyroshock wave measurement and simulation for space systems. Measurement: Journal of the International Measurement Confederation, 45(4), 631–642.

[11] NASA. (2011). Mitigating In-Space Charging Effects - A Guideline (NASA-STD-4002A).

[12] Institute of Environmental Sciences and Technology. (2009). Pyroshock Testing Techniques (IEST-RP-DTE032). Schamburg, IL: IEST.

[13] Biot, Maurice A. (1932) Transient Oscillations in Elastic Systems. Dissertation (Ph.D.), California Institute of Technology, Pasadena, CA.

[14] Irvine, B. T. (2012). An introduction to the shock response spectrum, Rev S. 1-73. Retrived from https://www.vibrationdata.com/tutorials2/srs_intr.pdf

[15] Lee, J., Hwang, D. H., & Han, J. H. (2018). Study on pyroshock propagation through plates with joints and washers. Aerospace Science and Technology, 79, 441–458.

[16] Park, H. S., Hwang, D. H., Han, J. H., & Yang, J. (2020). Development of shock-absorbing insert for honeycomb sandwich panel. Aerospace Science and Technology, 104, 105930.

[17] Cui, D., Zhao, J., Yan, S., Guo, X., & Li, J. (2015). Analysis of parameter sensitivity on dynamics of satellite separation. Acta Astronautica, 114, 22–33.

[18] Zhao, H., Hao, Z., Liu, W., Ding, J., Sun, Y., Zhang, Q., & Liu, Y. (2019). The shock environment prediction of satellite in the process of satellite-rocket separation. Acta Astronautica, 159(July 2018), 112–122.

[19] García-Pérez, A., Ravanbakhsh, A., Sorribes-Palmer, F., & Alonso, G. (2020). Structural shock verification by numerical analysis of the EPD payload units on board Solar Orbiter spacecraft. Acta Astronautica, 168(July 2019), 282–292.

[20] García-Pérez, A., Sorribes-Palmer, F., Alonso, G., & Ravanbakhsh, A. (2019). FEM simulation of space instruments subjected to shock tests by mechanical impact. International Journal of Impact Engineering, 126(November 2018), 11–26.

[21] Hwang, D. H., Park, H. S., & Han, J. H. (2020). Development of a miniature point source pyroshock simulator. Journal of Sound and Vibration, 481, 115438.

[22] Yan, H., Qin, Z., Zhang, W., Ming, A., Wang, X., & Chu, F. (2019). Dynamic analysis of laser shock response: Experimental and numerical studies. Aerospace Science and Technology, 94, 105430.

[23] Zhao, H., Liu, W., Ding, J., Sun, Y., Li, X., & Liu, Y. (2018). Numerical study on separation shock characteristics of pyrotechnic separation nuts. Acta Astronautica, 151(June), 893–903.

[24] Stewart, L. K., Durant, B., Wolfson, J., & Hegemier, G. A. (2014). Experimentally generated high-g shock loads using Hydraulic Blast Simulator. International Journal of Impact Engineering, 69, 86–94.

[25] Monti, R., & Gasbarri, P. (2017). Dynamic load synthesis for shock numerical simulation in space structure design. Acta Astronautica, 137(January), 222–231.

[26] Wang, X., Qin, Z., Ding, J., & Chu, F. (2017). Finite element modeling and pyroshock response analysis of separation nuts. Aerospace Science and Technology, 68, 380–390.

[27] García-Pérez, A., Sorribes-Palmer, F., Alonso, G., & Ravanbakhsh, A. (2018). Overview and application of FEM methods for shock analysis in space instruments. Aerospace Science and Technology, 80, 572–586.

[28] Siam, N. (2010). Development of an efficient analysis method for prediction and structural dimensioning of space structures subjected to shock loading (Master's Thesis). Luleå University of Technology, Noordwijk.

[29] Dilhan, D., Cipolla, V. (2005, May 10-12). Pyroshock Generation. [Conference Presentation]. European Conference on Spacecraft Structures, Materials and Mechanical Testing, Noordwijk, The Netherlands.

[30] Jonsson, M. (2012). Development of a shock test facility for qualification of

space equipment (Master's Thesis). Chalmers University of Technology, Göteborg, Sweden.

[31] Eriksson, J., Hansson, M. (1999). Measuring and analysis of pyrotechnic shock. Chalmers University of Technology, Göteborg, Sweden.

[32] Harris, C. M., & Piersol, A. G. (2010). Harris' Shock and Vibration Handbook 6th Edition. New York, NY: The McGraw-Hill Companies, Inc.

[33] Ott, R. J., & Folkman, S. (2017). Full-scale pyroshock separation test: Attenuation with distance. Journal of Spacecraft and Rockets, 54(3), 602–608.

[34] Hautaluoma, G., Edwards, A., Kanigan, D., and Patterson, T. (2009). Test in Development of NASA's New Crew Rocket is Successful. http://www.nasa.gov/mission_pages/constellation/ares/flighttests/aresIx/skirt_test.html [retrieved 22 Nov. 2020].

[35] Zhou, C. Y., Yu, T. X., & Suhir, E. (2009). Design of shock table tests to mimic real-life drop conditions. IEEE Transactions on Components and Packaging Technologies, 32(4), 832–837.

[36] Dilhan, D., Piquereau, A., Bonnes, L., and Van de Veire, J. (2008). Definition and manufacturing of the pyroshock bench. Proceedings of the 7th ESA/CNES International Workshop on Space Pyrotechnics, Noordwijk, Netherlands.

[37] Charvet, B., Dilhan, D., Palladino, M. (2014). Shock Bench Enhancements. Proceedings of the 13th European Conference on Spacecraft Structures, Materials & Environmental Testing, Braunschweig, Germany.

[38] Harris, C. M., & Piersol, A. G. (2002). Harris' Shock and Vibration Handbook 5th Edition. New York, NY: The McGraw-Hill Companies, Inc.

[39] Chong, S. Y., & Lee, J. R. (2014). Pointwise Explosive-Induced Pyroshock Wave Prediction Based on Numerical Conditioning of Laser Shocks. Experimental Mechanics, 54(9), 1651–1671.

[40] Zhao, H., Ding, J., Zhu, W., Sun, Y., & Liu, Y. (2019). Shock response prediction of the typical structure in spacecraft based on the hybrid modeling techniques. Aerospace Science and Technology, 89, 460–467.

[41] de Benedetti, M., Garofalo, G., Zumpano, M., & Barboni, R. (2007). On the damping effect due to bolted junctions in space structures subjected to pyro-shock. Acta Astronautica, 60(12), 947-956.

[42] NASA. (2001). Dynamic Environmental Criteria (NASA-STD-7005).

[43] Lee, D.-O., Han, J.-H., Jang, H.-W., Woo, S.-H., & Kim, K.-W. (2010). Shock Response Prediction of a Low Altitude Earth Observation Satellite During Launch Vehicle Separation. International Journal of Aeronautical and Space Sciences, 11(1), 49-57.

[44] Yan, Y., Li, P., Lin, H. (2016). Analysis and experimental validation of the middle-frequency vibro-acoustic coupling property for aircraft structural model based on the wave coupling hybrid FE-SEA method. Journal of Sound and Vibration, 371, 227–236.

[45] Luo, W., Cheng, L., Tong, L., Yu, W., Mechefske, C. (2018). Prediction and analysis of structural noise from a U-beam using the FE-SEA hybrid method. Promet-Traffic Transport, 30(3) 333–342.

[46] Troclet, B., Hiverniau, B., Ichchou, M., Jezequel, L., Kayvantash, K., Bekkour, T., Mouillet, J., Gallet, A. (2009). FEM/SEA hybrid method for predicting mid and high frequency structure-borne transmission. The Open Acoustic Journal, 2, 45-60.

[47] Zukas J. A. (2004). Introduction to Hydrocodes 1st edition. Elsevier Science.